(2)

AD-A237 466

REPORT DOCUMENTATION PAGE

1a.	1b. RESTRICTIVE MARKINGS: N/A
2a.	3. DISTRIBUTION / AVAILABILITY OF REPORT: Approved for public release; distribution unlimited.
2b. DECLASSIFICATION / DOWNGRADING SCHEDULE: N/A	
4. PERFORMING ORGANIZATION REPORT NUMBER(S): N00014-89-J-1314- 13	5. MONITORING ORGANIZATION REPORT NUMBER(S)
6a. NAME OF PERFORMING ORGANIZATION: LASST, University of Maine	6b. OFFICE SYMBOL (If applicable)
7a. NAME OF MONITORING ORGANIZATION: Office of Naval Research, Branch Office Chicago	
6c. ADDRESS (City, State, and ZIP Code): Sawyer Research Center, Orono, ME 04469	7b. ADDRESS (City, State, and ZIP Code): 536 S. Clark Street, Chicago, IL 60605
8a. NAME OF FUNDING/SPONSORING ORGANIZATION: Office of Naval Research--Chemistry Program	8b. OFFICE SYMBOL (If applicable)
9. PROCUREMENT INSTRUMENT IDENTIFICATION NUMBER: N00014-89-J-1314	
8c. ADDRESS (City, State, and ZIP Code): 800 N. Quincy Street, Arlington, VA 22217	10. SOURCE OF FUNDING NUMBERS: PROGRAM ELEMENT NO. / PROJECT NO. / TASK NO. / WORK UNIT ACCESSION

11. TITLE (Include Security Classification): Surface Structure and Surface Order

12. PERSONAL AUTHOR(S): W. N. Unertl

13a. TYPE OF REPORT	13b. TIME COVERED	14. DATE OF REPORT (Year, Month, Day)	15. PAGE COUNT
Technical	FROM 1/6/90 TO 31/5/91	15 May 1991	79

16. SUPPLEMENTARY NOTATION: To be published as Chapter Six in "Scanning Tunneling Microscopy", Ed. D. A. Bonnell (VCH Pub., New York, 1991)

17. COSATI CODES		
FIELD	GROUP	SUB-GROUP

18. SUBJECT TERMS (Continue on reverse if necessary and identify by block number): Crystallography, Phase Transitions

19. ABSTRACT (Continue on reverse if necessary and identify by block number)

This book chapter provides an introduction to the current state of knowledge about the crystal structure of solid surfaces, phase transitions on surfaces, and defects on surfaces.

20. DISTRIBUTION / AVAILABILITY OF ABSTRACT: ☐ UNCLASSIFIED/UNLIMITED ☒ SAME AS RPT. ☐ DTIC USERS	21. ABSTRACT SECURITY CLASSIFICATION: unclassified
22a. NAME OF RESPONSIBLE INDIVIDUAL: William N. Unertl	22b. TELEPHONE (Include Area Code): 207-581-2251 / 22c. OFFICE SYMBOL

DD FORM 1473, 84 MAR — 83 APR edition may be used until exhausted. SECURITY CLASSIFICATION OF THIS PAGE

CHAPTER FIVE

SURFACE STRUCTURE AND SURFACE ORDER

by

W. N. Unertl

Laboratory for Surface Science and Technology

University of Maine

Prepared for the book

SCANNING TUNNELING MICROSCOPY

Edited by D. A. Bonnell

The spatial arrangements of atoms near surfaces and interfaces determine the chemical, electronic and mechanical properties of materials in ways that cannot be simply predicted from a knowledge of bulk properties. For example, processes such as epitaxial growth of thin films and catalytic reactions are sensitive functions of surface structure and composition.

Most of our knowledge about surfaces has been acquired from studies of the surfaces of highly crystalline metals and semiconductors. Consequently, these materials are fairly well understood. However, significant gaps remain in understanding of other materials and, in particular, real surfaces such as those of non-crystalline materials like polymers. The surface properties of oxides and carbides are dominated by the presence of defects and are only beginning to be understood. Furthermore, real surfaces are often formed in metastable structural states rather than in thermodynamic equilibrium. With the recent introduction of direct imaging techniques like scanning tunneling microscopy (STM) and low energy electron microscopy (LEEM), there has been a rapid increase in research directed toward understanding the noncrystalline aspects of surface structure. Surface defects range from atomic scale defects such as impurities and vacancies to macroscopic imperfections such as grain boundaries. Diffusion, nucleation, growth, and chemical reactivity are sensitive to the presence of surface defects of both mesoscopic and microscopic extent. This chapter places more emphasis on surface defects than can be found in most other introductory discussions of surface structure. The reader is assumed to be familiar with the basic concepts of bulk thermodynamics, bulk crystallography, and bulk condensed matter physics [1].

6.1. IDEAL SURFACES OF CRYSTALLINE MATERIALS

We begin with a useful conceptual model - the *ideal surface*. Ideal surfaces have translational symmetry in directions parallel to the surface and contain no imperfections.

The simplest ideal surfaces are called *singular surfaces*. They have the structures that would form if a perfect bulk crystal could be cut to expose the atoms of an {hkl} plane at the surface without allowing them to adjust to their

new environment by relaxing from their bulk positions. Because their atoms have the same arrangement as bulk planes, singular surfaces are also called (1 x 1) surfaces. Singular surfaces do not exist in nature but the structures of the close-packed surfaces of many face-centered-cubic (fcc) and body-centered-cubic (bcc) metals have lateral structures that are nearly singular. A singular surface is identified by its Miller indices (hkl). As examples, fig. 6.1 shows

Figure 6.1. Structural models of low index singular surfaces of fcc and bcc crystals. The unfilled circles represent atoms in the surface layer, the lightly shaded circles are atoms in the second layer, and the dark circles are atoms in the third layer. The arrows indicate directions in each surface.

geometrical models of the (111), (110), and (100) surfaces of fcc and bcc crystals. In the case of fcc surfaces, the density of surface atoms is highest for (111), lower for (100), and lowest for (110). For bcc surfaces the (110) surface is most densely packed, (100) is more open, and (111) is very open - atoms in the third layer are exposed. Determination of the singular surface structures of other crystal types such as the diamond and hexagonal-close-packed (hcp) lattices is left as an exercise.

The structure of an (hkl) singular surface is classified according to its *two-dimensional Bravais lattice* type. A two dimensional Bravais lattice consists of an infinite planar array of points, each of which can be transformed into any other by the translation operator

$$\mathbf{T} = h\mathbf{a}_1 + k\mathbf{a}_2 \qquad (1)$$

where h and k are the two-dimensional Miller indices. The surface analogue of the bulk unit cell is the *unit mesh*: it is defined by its unit mesh vectors $\mathbf{a}_1$ and $\mathbf{a}_2$. Figure 6.2 shows the unit meshes of the five possible Bravais lattices

Figure 6.2. The five two dimensional Bravais Lattices. The angle β should always chosen to be greater than 90°.

which, when combined with T, have the property that they can completely cover a plane. The set of individual atoms located inside each unit mesh is called the *basis* of the surface structure. Although it is not necessary to choose the coordinate system so that one of the atoms of the basis coincides with the origin, it is often convenient to do so. In the case of the simple surface structures shown in fig. 6.1, each basis consists of a single atom. More complex structures are also common. For example, the (100) surface of the NaCl structure, fig. 6.3, has a two atom basis - in this case chosen with one

Figure 6.3. The (100) surface of a crystal with the NaCl structure. The primitive unit mesh is outlined in the upper left corner.

atom at the origin of the unit mesh and the other at its center. The distribution of atoms in the unit mesh may also have additional symmetry properties under 1-, 2-, 3-, 4-, and 6-fold rotations, reflections, and glide lines. However, it can be proved that there are only 17 unique combinations of these symmetry operations with the five Bravais lattices; these are called the two dimensional space groups [2]. In other words, all possible surface crystal structures must belong to one of these 17 space groups.

6.1 a. Relaxations

Atoms near a surface are located in very asymmetric environments. Thus, the bulk positions no longer correspond to the lowest energy state. This drives the surface atoms into new locations that correspond to the state of minimum free energy. In the simplest cases, only small displacements from singular positions are needed to achieve the equilibrium structure. The most common displacement is *relaxation*. In this case, the structure of each plane of atoms parallel to the surface remains singular, but the spacings between the outermost few planes change from the bulk value.

In cases such as inert gas crystals, where the forces between atoms can be accurately approximated by pairwise central potentials, the interplanar relaxation is always an expansion. The outermost layer of atoms is most

strongly affected and expansions of several percent are common [3]. The magnitude of the expansion decays to zero within a few layers.

Inward relaxations, or contractions, of the interplanar spacing also occur, especially for more open surface structures such as the (110) surfaces of fcc metals. Detailed experimental studies show that the interplanar spacings near a (110) surface decay in an oscillatory manner for at least three layers. The spacing between the first and second layers is contracted by δ_{12} whereas that between the second and third layers is expanded by δ_{23} which has smaller magnitude; i.e. $|\delta_{12}| > |\delta_{23}|$. Values of δ_{12} and δ_{23} have been measured for Al(110), Cu(110), and Cu(100) [4].

For contractions to be possible, the interatomic potentials must vary near the surface. One cause of variation is due to a redistribution of electrons. Finnis and Heine [5] developed the simple model illustrated in fig. 6.4 to

Figure 6.4. The Finnis-Heine model for surface contraction. (a) The surface created by maintaining the bulk charge distribution around each ion at the surface. Each square is a bulk Wigner-Seitz cell. (b) Redistribution of the conduction electrons to smooth the surface. The ion cores are still in their bulk locations. (c) Inward displacement of the ion cores to a position of equilibrium.

demonstrate how such a redistribution causes contraction. Far from the surface, the conduction electrons are symmetrically distributed inside each Wigner-Seitz cell and they screen the ion cores resulting in a net attractive interaction between neighboring cells. If this arrangement is assumed to extend right up to the surface as shown in fig. 6.4a, the electrons would be in a highly unfavorable environment. They lower their kinetic energy by smoothing the surface as in fig. 6.4b. This creates an asymmetrical electron distribution that produces a net inward force on the ion cores and causes them to move toward the bulk and thereby decrease the interatomic spacing (fig. 6.4c). Landman, Hill, and Mostoller [6] have extended the model of Finnis and Heine to include a realistic electron-ion interaction and a self-consistent

electron density profile at the surface. Their calculations confirm that the relaxation should be oscillatory [7].

6.1 b. Structures Due to Adsorption and Segregation

When atoms or molecules are placed on a surface either by adsorption from a gas phase or by segregation from the underlying bulk phase, it is very common for highly ordered two dimensional crystalline structures to be formed. This was noted in 1927 in the original surface structure studies of Davison and Germer [8]. Often the adsorbed species form a separate layer on top of substrate atoms; fig. 6.5a shows a ball model example

Figure 6.5. Examples of ordered overlayer structures. (a) Ni(111)-(2 x 2)-H. (b) Ti(100)-(1 x 3)-O. (c)Ti(001)-(1 x 1)-N.

for H adsorbed on the Ni(111) surface [9]. In other cases, such as O adsorbed on Ta(100) , fig. 6.5b, the adsorbed atoms can mix into the top layer of the substrate [10] or, as is the case for N on Ti(001), fig. 6.5c, even form a new layer below the surface [11]. In other systems, adsorption causes major structural changes in the substrate atoms. Hydrogen adsorption on Ni(110) is one example [12].

The amount of a foreign material adsorbed onto a surface is expressed as a *coverage* Θ where Θ is usually defined as the number of adsorbed atoms or molecules per unit area divided by the number of substrate surface atoms per unit area of the clean surface. Using this convention, the H coverage in fig. 6.5a is $\Theta = 0.25$ and the O coverage in fig. 6.5b is $\Theta = 1/3$.

As for the clean surface, the structure of any ordered overlayer can be characterized by its two dimensional Bravais lattice (fig. 6.2), its unit mesh vectors $\mathbf{b}_1$ and $\mathbf{b}_2$, and by the positions of the atoms within the unit mesh. An overlayer unit mesh is normally defined with respect to the unit mesh ($\mathbf{a}_1$, $\mathbf{a}_2$) of the substrate surface. Overlayer unit mesh vectors are illustrated in fig. 6.5a for the H on Ni structure. In simple cases, like fig. 6.5a, for which the angle between $\mathbf{b}_1$ and $\mathbf{b}_2$ is the same as the angle between $\mathbf{a}_1$ and $\mathbf{a}_2$, a notation developed by Elizabeth A. Wood is used [13]. The general form for this

notation for an adsorbate Q on the (hkl) surface of substrate A with overlayer mesh vectors $|\mathbf{b}_1| = n|\mathbf{a}_1|$ and $|\mathbf{b}_2| = m|\mathbf{a}_2|$, is

$$A(hkl)\text{-}(n \times m)R(\theta)\text{-}Q \qquad (2)$$

where $R(\theta)$ indicates the angle θ (measured in degrees) between $\mathbf{b}_1$ and $\mathbf{a}_1$. If θ is zero, the $R(\theta)$ term is dropped. The structure in fig. 6.5a is thus denoted as a Ni(111)-(2 x 2)-H structure with a two atom basis. A few other examples of the Wood notation are shown in fig. 6.6. Figure 6.6a is an overlayer on a

Figure 6.6. Examples of overlayer unit meshes. (a) ($\sqrt{5}$ x $\sqrt{5}$)R(26.57) on a square substrate; (b) *c*(2 x 2) or ($\sqrt{2}$ x $\sqrt{2}$)R(45) on a square lattice; (c) A (2,1;0,2) structure with no Wood equivalent.

square substrate mesh such as the (100) surface of an f.c.c. or b.c.c. material. It has $|\mathbf{b}_1| = \sqrt{5}|\mathbf{a}_1|$, $|\mathbf{b}_2| = \sqrt{5}|\mathbf{a}_2|$, and $\theta = 26.57$ degrees so that its Wood notation is ($\sqrt{5}$ x $\sqrt{5}$)R(26.57). Some structures have several forms in the Wood notation. The one most often encountered in practice is shown in fig. 6.6b. The mesh on the left is a *c*(2 x 2) mesh where the *c* indicates a centered structure. The mesh on the right is ($\sqrt{2}$ x $\sqrt{2}$)R(45). It is left as an exercise to show that the notation for the structure in fig. 6.5b is Ta(100)-(1 x 3)-O and that for fig. 6.5c is Ti(001)-(1 x 1)-N.

The overlayer lattice in fig. 6.6c cannot be described by the Wood notation since the angle between $\mathbf{b}_1$ and $\mathbf{b}_2$ is not equal to that between $\mathbf{a}_1$ and $\mathbf{a}_2$. A second, more general notation which includes cases like fig. 6.6.c and is also more useful in making transformations between real space and reciprocal space representations is the matrix notation originally proposed by Park and Madden [14]. Since

$$\mathbf{b}_1 = m_{11}\mathbf{a}_1 + m_{12}\mathbf{a}_2 \qquad (3a)$$

and

$$\mathbf{b}_2 = m_{21}\mathbf{a}_1 + m_{22}\mathbf{a}_2, \qquad (3b)$$

every overlayer mesh can be described by the matrix

$$M = (m_{11}, m_{12}; m_{21}, m_{22}). \quad (4)$$

Only the primitive unit meshes are used in the matrix notation and the determinant of M is always a positive number equal to the ratio of the overlayer mesh area to the substrate mesh area. Each of the meshes in fig. 6.5 can be described using the matrix notation. For the ($\sqrt{5}$ x $\sqrt{5}$)R(26.57) lattice, fig. 6.6a, M = (2, 1; -1, 2) and det M = 5. For the c(2 x 2) lattice of fig. 6.6b, M = (1, 1; -1, 1) and det M = 2. Each of these three meshes is an example of a *Simple Lattice*. Simple lattices are those for which each element of M is an integer and the determinant of M is an integer. Simple lattices have the property that if one lattice site of the overlayer coincides with a substrate lattice site then so do all other overlayer lattice sites. Simple lattices often occur when a single type of adsorption site is occupied by the adsorbed species and when the interaction between the adsorbate and the substrate is stronger than the adsorbate-adsorbate interaction. Many atoms and molecules adsorb at sites on the substrate that have high symmetry; fig. 6.7 shows models of the

Figure 6.7. Various types of adsorption sites on the low index fcc and bcc surfaces of fig. 6.1. The black dots represent adsorbed atoms. Sites labeled OT are on-top adsorption. Hollow sites with high symmetry are indicated by H. Bridge sites are indicated by B if all possible sites are the same, otherwise there are long-bridge LB and short-bridge SB sites depending on the relative distance between the substrate atoms.

important high symmetry adsorption sites on bcc and fcc surfaces. The more densely packed surfaces have fewer types of high symmetry sites whereas open surfaces like the bcc (111) have a wider variety.

Another class of overlayer lattices are the *coincidence lattices* for which some of the elements of M are rational numbers and det M is a simple fraction. At coverages near 0.67 monolayer, a (1.5, 0; 0.5, 1) coincidence structure occurs for N_2 adsorption on a Ni(110) surface [15]. Figure 6.8 shows the unit

Figure 6.8. A (1.5, 0; 0.5, 1) structure. The adsorbate molecules occupy both on-top and short-bridge sites.

mesh of this structure. Coincidence lattices have the property that there is no orientation of the overlayer for which every overlayer lattice point coincides with a substrate lattice point. Coincidence lattices can occur when several types of adsorption site are simultaneously occupied or when adatom-adatom interactions are of comparable strength to adatom-substrate interactions.

The third class of overlayer structures are *incoherent* or *incommensurate lattices*. In this class some elements of M and det M are irrational numbers. Incommensurate lattices are typically formed when the interaction between the adsorbate atoms is stronger than their interaction with the substrate and are often observed for submonolayers of inert gases.

It is important to realize that neither the Wood notation nor the matrix notation contain any information about either the number of atoms or their locations within the unit mesh. This information must be obtained from detailed structure determinations. A large fraction of the research in the area of surface crystallography has been devoted to the development of improved techniques and their application to more and more complex structures. Atom locations are usually extracted from the data assuming that the surface is free of defects and imperfections. Current technology can determine interatomic bond lengths to a precision of about 0.01 nm or better. The bond lengths at surfaces typically lie within the range observed for similar bonds in molecular and bulk compounds as demonstrated in fig. 6.9. Several compilations of surface structures are available [7,16].

Figure 6.9. Comparison of bond lengths for surface structures (arrows) with ranges of bond lengths found in bulk compounds and molecules (boxes). After reference 7.

6.1 c. Reconstructions

Many clean surfaces take on structures that differ substantially from the ones predicted from the underlying bulk structure. Such surfaces are said to be *reconstructed*. The (7 x 7) reconstruction of Si(111) is probably the most well

known and complicated example of a reconstructed surface and is shown in fig. __. Simpler reconstructions also occur. For the (100) surface of Ir, the surface atoms form a nearly hexagonal (111) layer which is slightly distorted by interactions with the underlying (100) layers [17]. Au(100) and Pt(100) have similar reconstructions. In these three examples, the atomic density of the surface layer is larger than in the bulk. For other reconstructions, like the (1 x 2) reconstruction of the (110) surfaces of Au, Pt, and Ir, the reconstructed layer has a reduced density [18-20]. The unreconstructed (110) surfaces of fcc materials consists of rows of close-packed atoms parallel to the [1,-1,0] direction as illustrated in fig. 6.1. Figure 6.10 shows an end-on view of a ball model of the reconstructed Au(110)-(1 x 2)

Figure 6.10. A ball model of the Au(110)-(1 x 2) reconstruction (after ref. 20). Arrows indicate the direction of shifts from singular positions.

surface. This type of (1 x 2) reconstruction is called a *missing row* structure because every other row of surface atoms has been removed. Reconstruction of the surface layer also causes subsurface atoms to shift from their singular positions, primarily by pairing of [1,-1,0] rows of atoms in the second layer, in response to the loss of neighbors in the surface layer.

Theoretical studies [21-23] of metal surface reconstruction show that d-electron interactions must be included in a realistic way to account for the experimental result that clean Au, Pt, and Ir (110) surfaces have the (1 x 2) reconstruction but Ag, Cu, and Ni do not. The models used are very sensitive to higher order contributions to the interatomic potential such as three body interactions and have not yet succeeded in calculating every detail of the structure such as the direction of displacements in the second layer.

Most surfaces of elemental and compound semiconductors are also reconstructed. Because bonds in semiconductors are more directed than in metals or ionic crystals, the major contribution made to the surface energy in forming a new piece of semiconductor surface, say by cleavage, is the energy required to break those bonds that cross the interface. These broken bonds are directed out of the surface and are called *dangling bonds*. The free energy of the surface can usually be lowered by reconstruction to a new structure in

which the number of broken bonds has been reduced. This process is called *rehybridization*. On the Si(100) surface rehybridization leads to the formation of symmetric dimers which lie on a (2 x 1) reconstructed lattice as illustrated in fig. 5.11. This book contains several other examples of semiconductor

Figure 6.11. An STM image of the Si(100)-(2 x 1) reconstruction [24]. Each number along the side marks a row of dimers. A unit mesh of the reconstructed surface is also shown. The surface region shown also has numerous defects.

reconstructions in Figs.____. Some reconstructions such as the Si(111)-(7 x 7) involve complex rearrangements of the uppermost several layers of atoms. Tight-binding methods have been developed to provide a semi-quantitative theoretical basis for many of the experimentally observed reconstructions [25].

Surface reconstructions can also be induced by adsorption. If CO is adsorbed on the clean Pt(110)-(1 x 2) surface, the missing row structure is destroyed. This process has been studied by Gritsch et al. [26] and one of their beautiful STM images illustrating an intermediate stage of the deconstruction of the (1 x 2) structure is shown in fig. 6.12. A second example of adsorption

Figure 6.12. The STM image on the left shows a "hole" induced in the reconstructed Pt(110)-(1 x 2) surface by the adsorption of CO [26]. The CO molecule is not visible in the image. A ball model is shown on the right.

induced changes in the surface structure of the substrate is provided by hydrogen adsorption on Ni(110) and Pd(110) surfaces. H_2 causes adjacent [1,-1,0] rows of surface metal atoms to move closer together and form a (1 x 2) "paired-row" structure [12, 27].

In some cases, extremely small changes in surface composition are sufficient to induce reconstructions. For example, very small amounts of alkali metal adsorbates ($\theta < 0.2$) cause the (110) surfaces of Cu and Ag to reconstruct into a (1 x 2) missing row structure [28]. For compounds or alloys such as

Cu_3Au, the equilibrium surface composition is often different from the bulk composition and this can lead to changes in surface order[29].

6.1 d. Surface Electronic Structure.

The electronic properties of surfaces are discussed in some detail in other portions of this book. In this chapter, we wish to point out that the atomic arraignment and the electronic properties of surfaces are intimately interrelated. If the atomic positions are altered, the electronic properties will also be changed and visa versa. The sensitivity of the surfaces of Cu(110) and Ag(110) to reconstruction in the presence of very small amounts of alkali metals mentioned above is probably caused by change in the electronic structure.

The importance of the coupling between the atomic and electronic structures is apparent in the Schrödinger equation for the many electron system:

$$H\,\psi_j(\mathbf{r},\mathbf{R}) = E_j\psi_j(\mathbf{r},\mathbf{R}) \tag{5}$$

where

$$H = \sum_{M=1}^{N-1}\left(\frac{-\hbar^2}{2m_M}\right)\nabla_M^2 + \sum_{i=1}^{n}\left(\frac{-\hbar^2}{2m}\right)\nabla_i^2 + \sum_{i=1}^{n-1}\sum_{j>i}^{n}\frac{e^2}{|\mathbf{r}_i - \mathbf{r}_j|} + \sum_{i=1}^{n}\sum_{M=1}^{N}\frac{e^2 Z_M}{|\mathbf{r}_i - \mathbf{R}_M|} + \sum_{M=1}^{N-1}\sum_{M'>M}^{N}\frac{e^2 Z_M Z_{M'}}{|\mathbf{R}_M - \mathbf{R}_{M'}|}\,.$$

Both the electronic wavefunctions $\psi_j(\mathbf{r},\mathbf{R})$ and the Hamiltonian H depend not only on the positions $\mathbf{r}_i$ of the electrons but also on the positions $\mathbf{R}_j$ and charges Z_M of the nuclei. The $\psi_j(\mathbf{r},\mathbf{R})$ for a given set of boundary conditions are determined by a self-consistent solution of eqn. 5. For real systems, this problem is most often too complex to be solved exactly but numerous, usually computer intensive, approximate methods have been developed [30].

This close relationship between the atomic positions and electronic properties of a surface is especially important for techniques like STM that measure electronic quantities and try to deduce the atomic structure from them. For example, certain atoms can appear in or disappear from an STM image

depending on the portions of the electronic density of states that are being sampled. This important point is discussed in detail in Chapters _____.

6.2. THERMODYNAMIC PROPERTIES OF SURFACES

6.2 a. Surface Energy and Surface Structure.

The reversible work required to form a unit area of new surface of a given orientation {hkl} at constant volume, temperature, and chemical potential μ_i of each of the components is called the *surface energy* γ(hkl). For solids, γ(hkl) lies in the range 0.1 J/m^2 to 2.5 J/m^2 [31,32]. The magnitude of γ(hkl) for an (hkl) surface is intimately related to its atomic structure; atoms near the surface have fewer neighbors and different geometrical configurations than atoms in the bulk.

Interatomic bonds form because they lower the internal energy U of the participating atoms. The magnitude of U can be estimated by considering a simple model with only nearest neighbor interactions of strength ε. The bond energy is shared between the atoms so that the internal energy of each atom is lowered by $\varepsilon/2$ for every bond it forms. For example, atoms at an fcc (111) surface have only nine nearest neighbors compared to twelve in the bulk. Each surface atom has three less bonds which results in an excess internal energy of $3(\varepsilon/2)$ per surface atom. An estimate of ε can be obtained from the latent heat of sublimation L_S since, if one mole of bulk solid is vaporized, $12N_A$ bonds are broken. Thus the internal energy per atom for a (111) surface is on the order of

$$U(111) \sim 0.25\ L_S/N_A. \qquad (6)$$

This crude model ignores interactions due to higher order neighbors, assumes that the value of ε is the same for surface and bulk atoms, and does not include entropic or pressure-volume contributions to γ(hkl); i. e.

$$\int_A \gamma(hkl)dA = U + PV - TS. \qquad (7)$$

None the less, it does account for the relative differences in γ(hkl) between different materials and for the fact that less dense surfaces of a material have lower γ(hkl).

Reliable measurements of γ(hkl) are difficult because even fractions of a monolayer of an impurity can change γ(hkl) by amounts which are larger than the variation between faces. Thus, accurate values are available for only a few materials. The effect of orientation and temperature on γ(hkl) is illustrated for the case of Pb in fig. 6.13.

Figure 6.13. γ(hkl) for lead at several temperatures [33]. The data are normalized to γ(111).

The equilibrium shape of a crystal in contact with its vapor at constant temperature and volume is that shape for which the total energy associated with the surface is minimized [32] and is given by the minimum of the integral

$$\int_A \gamma(hkl)dA. \qquad (8)$$

At low temperatures, the equilibrium shapes are regular polyhedra whose facets are made up of low index surfaces such as {111} and {100}. It seems that the edges at the intersection of two facets can be either sharp or rounded but only a few reliable measurements are available. Since γ(hkl) changes with temperature, the fraction of the surface due to a particular {hkl} will also change with temperature. Nearer the melting point, as can be seen from fig. 6.13, the differences in γ(hkl) for nearby {hkl} are reduced and large regions of curved surface are possible. In the case of Pb near its melting point, fig. 6.14, the equilibrium shape is nearly spherical; there are no {110} facets and

Figure 6.14. Scanning electron micrographs of a small Pb crystal. (a) Near its melting point; T = 599 K [34]. The larger flat facets are {111} surfaces and the smaller ones are {100} surfaces. (b) A slightly larger crystal showing the increase in surface topographical structures that occurs at lower temperature; T = 373 K. (Courtesy of A. Pavlovska).

only small {111} and {100} facets. For liquids, atoms are no longer fixed at crystalline sites so that each point on the surface will have the minimum value of γ; i.e. γ has no angular dependence and the equilibrium shape is a sphere.

6.2 b. Phase Diagrams

The ordered overlayer structures and reconstructed surfaces discussed above are examples of discrete surface phases. In addition to crystalline phases, it is also common to observe liquid, and gaseous phases. Each surface phase is stable over only a limited range of thermodynamic variables such as temperature, coverage, or gas pressure. The range of thermodynamic parameters over which any phase can exist in thermodynamic equilibrium is conveniently summarized in a *phase diagram*, such as that for O adsorbed on Ni(111), shown in fig. 6.15 [35]. The ranges of T and Θ over which each of

Figure. 6.15. Equilibrium phase diagram for O-Ni(111) [35].

the various phases exist are delineated by lines called phase boundaries. The regions labeled *Gas*, *p(2 x 2)*, and *($\sqrt{3}$ x$\sqrt{3}$)R(30)* in which only one phase occurs are called *single*, or *pure*, phase regions. If two phases are present simultaneously, the region is called a *coexistence* region. The regions labeled *p(2 x 2) + Gas* and *p(2 x 2) Antiphase Domains + Liquid* in fig. 6.15 are examples of coexistence regions. The phase diagram for Se-Ni(100) is shown in fig. 6.16 [36].

Figure 6.16. (a) The equilibrium phase diagram for Se-Ni(100) [36]. (b) Structure of the p(2 x 2) phase. (c) Structure of the c(2 x 2) phase The solid circles are Ni atoms and the open circles are Se atoms. (d) Interactions between Se atoms at various separations.

The O-Ni(111) system can be considered to be a *closed system*: i. e. the O coverage is independent of temperature because O atoms are so strongly bound to the Ni substrate that thermally activated desorption is insignificant

over the temperature range covered by the phase diagram. At higher temperatures, the adsorbed atoms could be desorbed into the gas phase, dissolved into the substrate, or react with the substrate to form new compounds. For the case of O-Ni(111), the latter occurs. In cases such as N_2 on Ni(110) [15] in which desorption occurs, constant coverage can often still be maintained if a gas phase of the adsorbate is maintained over the sample. This is impractical for other systems such as Se-Ni(100); in these cases desorption limits the highest temperature, T_m, at which an equilibrium phase diagram can be measured. T_m is determined primarily by $E_D(\Theta)$, the coverage dependent activation energy required to desorb an atom or molecule; E_D can range from a few meV for weakly bound adsorbates like the inert gasses up to several eV for very reactive adsorbates. The rate of desorption can be estimated from

$$d\Theta/dt = \nu \exp(-E_D/kT) \qquad (9)$$

where k is the Boltzmann constant and the pre-exponential term ν depends upon the detailed desorption mechanism and the attempt frequency. Typically, is assumed to be on the order of the a vibration frequency ($\sim 10^{13}$ s^{-1}) [37]. There are also practical lower temperatures for which phase equilibrium can be studied because kinetic processes such as diffusion become too slow for equilibrium to be reached within a practical time interval. Phase diagrams for closed systems are determined by measuring the structure as a function of T and Θ. In the case of weakly bound adsorbates, the chemical potential, and thus the coverage of the system, is controlled by the pressure of the gas phase. Phase diagrams for these *open systems* are usually determined by measuring the surface structure as a function of the substrate temperature and the gas pressure with the gas phase at room temperature.

The crystallographic structure of each phase and the precise locations of its phase boundaries are determined by the interactions of the adsorbate atoms with each other and with substrate atoms. If the structures of the phases are known, the sequence in which they form as Θ is increased provides direct information about the relative interaction strengths between pairs of adsorbate atoms on various possible adsorption sites. For example, fig. 6.16 shows the phase diagram for Se adsorbed on Ni(100) and the atomic structures of the p(2

x 2) and c(2 x 2) phases. The figure also defines the interaction energies between Se adsorbed on first, second, and third nearest neighbor sites. In the p(2 x 2) phase, first and second nearest neighbor sites are not occupied by Se. Therefore, the interaction E_3 must be more attractive than E_1 or E_2. Since the c(2 x 2) phase forms next, E_2 must be more attractive than E_1. Thus, $E_3 < E_2 < E_3$. The numerical values of these energies can be estimated using various statistical mechanical techniques in which the values of the E_i are adjusted until an acceptable fit to the measured phase boundaries is obtained [38].

A limit to the maximum number of phases p that can coexist on a surface is given by the Gibbs' phase rule [39]. The number of independent variables or the number of degrees of freedom f for a system with c components and p phases is

$$f = c - p + 2. \qquad (10)$$

In the examples of Figs. 6.15 and 6.16, c = 1. Therefore, in single phase regions (p = 1) like the p(2 x 2) and c(2 x 2) phases, f = 2. This result means that there are two independent variables for each of these phases; in this case they are T and Θ. At the phase boundary between two phases (p = 2), f = 1. Thus, once either Θ or T is fixed, the other is uniquely determined. Three phases can only occur for unique value of T and Θ since f = 0. The Gibbs' phase rule is especially useful in constructing phase diagrams from experimental data since it is usually impractical to characterize a system at every point in its phase diagram.

6.2 c. Phase Transitions

The structure of a surface is profoundly changed whenever it undergoes a transition between two phases. Furthermore, the structural changes induced by the phase transition cause changes in other important physical and chemical properties such as mass transport and reactivity.

One useful classification of phase transitions is based upon the properties of the Gibbs free energy

$$G = U + PV - TS + \gamma A = H - TS + \gamma A = \Sigma \mu_i N_i \qquad (11)$$

where H is the enthalpy, A is the surface area, N_i the number of moles of component i, and μ_i the chemical potential of component i. A transition is said to be *first order* if any of the first derivatives of G - e. g. $\partial G/\partial T)_{P,N,A}$ and $\partial G/\partial P)_{T,N,A}$ - are discontinuous, as illustrated in fig. 6.17a. Since, from the

Figure 6.17. Temperature dependence of the Gibbs free energy G and the enthalpy H for (A) a first-order phase transition and (B) a second order phase transition.

combined first and second laws of thermodynamics

$$dG = VdP - SdT + \Sigma\, \mu_i dN_i + \gamma dA, \qquad (12)$$

$\partial G/\partial T)_{P,N,A} = -S$, $\partial G/\partial P)_{T,N,A} = V$, etc., first order transitions have discontinuous changes in V, S, μ_i, and γ. First order transitions also have a latent heat of transformation ΔH because the enthalpy, $H = U + PV$, is also discontinuous at the transition. The crystal structure also changes abruptly and every region of the surface is distinctly in one phase or the other. Fig. 6.18

Figure 6.18. (a) Coexisting regions of (7 x 7) and (1 x 1) phases on a slightly stepped Si(111) surface [40]. The dark areas are (7 x 7) and the light regions are (1 x 1). (b) Schematic illustration of the structure along the line AB in (a). (Courtesy of Y. Yagi.)

shows a reflection electron microscope image recorded during the first order (1 x 1) - to - (7 x 7) transition on the Si(111) surface [40]. The dark regions have already transformed to the (7 x 7) phase and the light regions are still in the (1 x 1) phase.

Second order phase transitions have continuous first derivatives of G but discontinuous second derivatives, fig. 6.17b. Thus, they have no latent heat. The concepts of symmetry and universality are central to the understanding of second order phase transitions between surface phases [41,42]. To understand

them, we begin with a discussion of how to quantify the degree of order in a surface.

Degree of Order in Surface Phases.

Surface order changes during a phase transition. Three measurable quantities that are used to measure this change are the order parameter ϕ, the pair correlation function $\langle n_i n_j \rangle$, and the correlation length ξ. These quantities can be defined in terms of a lattice gas of particles adsorbed on a lattice described by unit mesh vectors $\mathbf{a}_1$ and $\mathbf{a}_2$ and having adsorption sites at positions $\mathbf{r}_i = m_{1i}\mathbf{a}_1 + m_{2i}\mathbf{a}_2$ where m_{1i} and m_{2i} are integers. In this model, n_i, the probability at any instant that a particular site $\mathbf{r}_i$ is occupied, is either one or zero; $n_i = 0,1$. The average occupation probability $\langle n_i \rangle$ is determined by the average of all possible configurations of the particles, each weighted by its statistical probability [43]. As the degree of order changes near a phase transition, $\langle n_i \rangle$ also changes.

The *order parameter* ϕ describes the average degree of order at each site on the lattice as a function of temperature and is therefore closely related to the structure of the surface. In simple cases ϕ can be a single quantity such as the average site occupation $\langle n_i \rangle$ or the magnetization. In more complex cases, ϕ is a set of functions ϕ_j. Diffraction techniques such as low energy electron diffraction or grazing incidence x-ray scattering are sensitive probes of the type and degree of surface order and, for this reason, are commonly used to study phase transitions [7,44]. In the case of diffraction, it is most convenient to define the ϕ_j in terms of the Fourier coefficients of the average site occupation probability $\langle n_i \rangle$. The number of components j of ϕ_j is equal to the number of terms in this expansion. Consider the example of a (2 x 1) structure on a square lattice which has a two component (vector) order parameter as shown in fig. 6.19. In this case, the (2 x 1) and (1 x 2) structures are symmetrically

Figure 6.19. (a) Two symmetry equivalent domains of a (2 x 1) structure on a square lattice. The domain boundary is marked by the dashed line. (b) The surface Brillouin zone for (a). The substrate reciprocal mesh vectors are $\mathbf{a}_1^*$ and $\mathbf{a}_2^*$. The zone center is at Γ. The reciprocal

lattice vectors $\mathbf{k}_1$ and $\mathbf{k}_2$ describe the order parameters of the two (2 x 1) domains. The wave vector $\mathbf{q}$ describes the order parameter of a c(2 x 2) structure.

equivalent and can coexist on the surface. Order parameters that describe these possibilities are

$$\phi_1 = N^{-1}\Sigma_j <n_j> e^{i\mathbf{k}_1 \cdot \mathbf{r}_j} \qquad (13a)$$

and

$$\phi_2 = N^{-1}\Sigma_j <n_j> e^{i\mathbf{k}_2 \cdot \mathbf{r}_j} \qquad (13b)$$

where N is the number of lattice sites, $\mathbf{k}_1 = \mathbf{a}_1^*/2$ and $\mathbf{k}_2 = \mathbf{a}_2^*/2$ are reciprocal lattice vectors characteristic of each possible (2 x 1) lattice as shown in fig. 6.19 b and $\mathbf{a}_1^*$ and $\mathbf{a}_2^*$ are the reciprocal lattice unit mesh vectors of the substrate. For a perfect (2 x 1) phase $\phi_1 = 1/2$ and $\phi_1 = 0$. A c(2 x 2) phase, fig. 6.6 b, is another possible structure on the same square substrate lattice. The single component (scalar) order parameter ϕ_3 for this structure is determined by the reciprocal vector $\mathbf{q}$,

$$\phi_3 = N^{-1}\Sigma_j <n_j> e^{i\mathbf{q} \cdot \mathbf{r}_j}. \qquad (13c)$$

The *pair correlation function* $<n_i n_j>$ gives the probability that the lattice sites at $\mathbf{r}_j$ and $\mathbf{r}_i$ are simultaneously occupied and therefore $<n_i n_j>$ provides more information about the details of the ordering than does ϕ. Since n_i can be written as a sum of its average value $<n_i>$ plus its instantaneous fluctuation δn_i from that average, one obtains

$$<n_i n_j> = <n_i>^2 + <\delta n_i \delta n_j>. \qquad (14)$$

The functional form of $<\delta n_i \delta n_j>$ for a system that contains some amount of disorder is such that $<\delta n_i \delta n_j>$ decreases as $\mathbf{r}_j$ and $\mathbf{r}_i$ become farther apart. The

length which characterizes this fall-off is called the *correlation length* ξ. ξ provides an important measure of the distance over which fluctuations from the average coverage $\langle n_i \rangle$ are correlated.

Diffraction from a Disordered Lattice

If a perfect two-dimensional lattice is illuminated by radiation with wave vector $\mathbf{k}_o$ ($|\mathbf{k}_o| = 2\pi/\lambda$, where λ is the wavelength), diffracted beams are observed only at values of the scattered wave vectors $\mathbf{k}$ that satisfy the Laue conditions [45]. If a phase transition is taking place on the lattice, disorder is introduced and intensity is removed from the diffracted beams and redistributed into other directions. In this situation, there are two components of the averaged intensity scattered from the lattice [46]:

$$I \propto I_{LRO} + \chi(S) \tag{15}$$

where $S \equiv \mathbf{k} - \mathbf{k}_o$ is the scattering vector. Only $S_\parallel$, $k_{o\parallel}$, and $k_\parallel$, the components of S, $\mathbf{k}_o$ and $\mathbf{k}$, which are parallel to the plane of the surface, are important. I_{LRO}, the first term in eqn. 15, is the intensity that would be obtained for the perfectly ordered surface with an atom at every adsorption site but reduced by the factor ϕ^2; i.e.,

$$I_{LRO} \equiv \phi^2 \, \delta(S_\parallel + G_{hk}) \tag{16}$$

where G_{hk} are the reciprocal lattice vectors of the two-dimensional Bravais lattice. $\chi(S)$, the second term in eqn. 15, is due to the fluctuations:

$$\chi(S) = \Sigma_{ij} \langle \delta n_i \delta n_j \rangle e^{iS \cdot r_{ij}}. \tag{17}$$

In analogy with magnetic systems, $\chi(S)$ is called the *susceptibility*. $\chi(S)$ is a peaked function and its half-width $\Delta S_\parallel(1/2)$ is inversely related to the correlation length ξ by

$$|\Delta S_\parallel(1/2)| = 2\pi/\xi. \tag{18}$$

For the case of continuous phase transitions, the susceptibility can usually approximated as a Lorentzian function [46]. $\chi(S) = 0$ if the surface is perfectly ordered.

Critical Exponents and Universality

The way in which I_{LRO} and $\chi(S)$ change in the vicinity of a second order phase transition can be described by a set of numbers ω called *critical exponents*. The values of the critical exponents do not depend on the details of the interatomic potentials but are determined entirely by the symmetry properties of the surface. A set of empirical rules relating the ω to the surface symmetry was developed by Landau and Lifshitz [47]. Originally it was hoped that there would be only one set of critical exponents [48]. Instead, because of the variety of symmetries that can occur, there turn out to be several distinct sets called *universality classes*. Once the universality class of a particular surface system is known, its behavior near a second order transition is completely determined; i.e. membership in a universality class is a necessary condition for any surface system to undergo a second order phase transition. If a system does not belong to a universality class, it is impossible for it to have a second order phase transition. Additionally, even if a system belongs to a universality class, its phase transitions can still turn out to be first order.

Each critical exponent predicts the variation of specific physical quantities near the critical temperature of the transition. For example, if F(T) is a quantity of interest such as the order parameter, its variation near the critical temperature T_c can be described by a power series expansion

$$F(t) \approx F_o|t|^{\omega} + \ldots \qquad (19)$$

where $t \equiv (T - T_c)/T_c$ is the reduced temperature and F_o is an amplitude. Higher order terms in eqn. 19 are usually unimportant as long as T is near enough to T_c. The most important universality classes for two-dimensional systems are listed in Table I along with the values of of their critical exponents.

TABLE I

The temperature dependence of the order parameter is described by the critical exponent β:

$$\phi(t) \approx \phi_o|t|^{\beta} + \ldots \qquad T < T_c \qquad (20a)$$
$$= 0. \qquad T > T_c \qquad (20b)$$

The exponents γ and ω describe the behavior of $\chi(\Delta S_{\parallel}, t)$, eqn. 15. The amplitude of the susceptibility $\chi(0, t)$ obeys

$$\chi(0, t) \approx \chi_o|t|^{\omega} + \ldots \qquad (21)$$

and the correlation length is given by

$$\xi(t) \approx \xi_o|t|^{-\gamma} + \ldots \qquad (22)$$

where ξ_o is of the order of a lattice spacing.

Figure 6.20 is a schematic illustration of the variation of I_{LRO} and

Figure 6.20. Effect of the critical exponents on the diffraction at a second order phase transition [49]. The upper portion shows I_{LRO} and the amplitude of the susceptibility $\chi(0,t)$. The lower portion shows the angular profiles of diffraction beams just below, at, and just above T_c.

$\chi(S_{\parallel},t)$, near T_c predicted by eqns. 20 - 22. I_{LRO} falls continuously to zero at T_c. $\chi(0, t)$ is singular at T_c and decreases smoothly on both sides. Far below T_c only the δ-function I_{LRO} contributes to the line profile. As T increases toward T_c, I_{LRO} decreases and $\chi(S_{\parallel}, t)$ becomes significant. At $T << T_c$, $\chi(S_{\parallel}, t)$ is low and broad but increases in magnitude and sharpens until at T_C it is the only contribution to the line profile. As T increases above T_c, $\chi(S_{\parallel}, t)$ again decreases and broadens. Thus, an accurate measurement of the diffraction line

profile as a function of temperature near T_c can be analyzed to obtain β, γ and ν.

The Au(110)-(1 x 2) reconstructed surface undergoes an order-disorder transition with critical temperature near 700 K. Symmetry arguments [41,50] demonstrate that this system should belong to the Ising universality class whose exponents are listed in Table I. Campuzano et al. studied this transition using diffraction [46]. Figure 6.21 shows their measurements of $\chi(0, t)$ along with

Figure 6.21. Critical behavior of the Au(110)-(1 x 2) order-disorder transition [46]. The upper graph corresponds to the upper portion of fig. 6.20 and shows the temperature dependence of I_{LRO} and $\chi(0, T)$. The lower curve show ln-ln plots of I_{LRO}, $\chi(0, t)$, and $\Delta S_{\parallel}(1/2)$ which are used to determine the critical exponents in Table II.

ln-ln plots of I_{LRO}, $\chi(0, t)$, and $\Delta S_{\parallel}(1/2)$ whose slopes determine the exponents β, γ, and ν. The results are listed in Table II along with experimental results

TABLE II

for several other reconstructed clean surfaces and chemisorbed overlayers. In the case of Au(110)-(1 x 2), experiment confirms that the transition is second order and belongs to the Ising universality class.

Other types of phase transitions

There are several other types of phase transitions. Here we discuss briefly surface premelting, roughening, and commensurate-incommensurate transitions.

In the *premelting transition*, layers of atoms near the surface melt at lower temperatures than the bulk melting temperature [51]. A widely used empirical relation originally proposed by Lindemann asserts that melting occurs when the root-mean-square thermal vibrational amplitude $\langle u^2 \rangle^{1/2}$ exceeds about ten percent of the interatomic spacing. Premelting occurs because the vibrational amplitudes of atoms near a solid surface are typically at

least fifty percent larger than for atoms in the bulk. The origin of this enhancement can be understood by examining a linear chain of balls each with mass m connected by springs with force constants κ. If a ball far from the end of the chain is displaced from its equilibrium position by Δx, it experiences a restoring force $F_b = -2\kappa\Delta x$. Its average kinetic energy is $(2\kappa)\langle u^2_b\rangle/2$ which, by classical equipartition of energy, is equal to kT/2 where k is the Boltzmann constant. Thus, $\langle u^2_b\rangle = kT/2\kappa$. On the other hand, balls at the end of the chain feel a restoring force of only $-\kappa T$ because they have neighbors on only one side. Therefore, these "surface" balls have a root-mean-square vibrational amplitude of $\langle u^2_s\rangle = kT/\kappa = 2\langle u^2_b\rangle$; i.e. twice the bulk value. This argument predicts that the surface layer will melt at about $0.7T_m$ and is qualitatively correct for real surfaces.

Premelting explains why a solid cannot be superheated above its melting point. There is no nucleation barrier to formation of the liquid phase because premelting has already created a nucleus from which the liquid phase can grow.

Theoretical calculations of premelting, such as the molecular dynamics simulations shown in fig. 6.22, show that surface melting is expected to be

Figure 6.22. A molecular dynamics simulation for a two-dimensional slab showing trajectories of the atoms [52]. The bulk melting point is $T_m = 0.415\varepsilon/k$. The upper panel is just below T_m and the lower panel is just above T_m. (Courtesy of F. Abraham.)

significant only at temperatures very near the melting point. The thickness of the melted layer exceeds a few monolayers only when T is within a few degrees of the melting temperature. In the upper panel of fig. 6.22, the temperature is $0.96T_m$. In the center of the slab, each atom follows a trajectory that remains near its low temperature equilibrium position. However, at either surface, the atoms are able to wander and essentially no crystalline order remains. In the lower panel, the temperature is $1.01T_m$; the slab has clearly lost both its long range and short range order and has melted. Premelting transitions are poorly understood and the available experimental studies indicate that there may actually be several types of premelting behavior.

The *roughening transition* is the name given to the spontaneous formation of steps on a surface and is initiated at the temperature T_R at which the free energy change $\Delta F = \Delta U - T\Delta S$ required to form a step becomes zero [53]. Atoms at a step edge have fewer nearest neighbors so that step formation requires that interatomic bonds be broken at an energy cost of ΔU per unit length of step. In a nearest neighbor model, the energy per bond is $\varepsilon/2$, and $\Delta U = \varepsilon/2a$ where a is the interatomic spacing along the step. Step formation also increases the entropy of the surface particularly if the step edge is not straight. It is this increase in entropy theat drives ΔF to zero. In order for the roughening transition to occur T_R must be lower than the melting temperature T_m. Thus, roughening only occurs for more open surfaces that have low ΔU; e. g. the (113) and (115) surfaces of fcc metals [54]. The roughening transition is distinct from premelting since the surface retains a high degree of short range order in the roughened phase. Roughening is important in crystal growth since the steps provide a high density of sites which provide a template for nucleation and growth.

The *commensurate-incommensurate transition* was originally described by Frank and van der Merwe [55]. This transition has been studied for a large number of systems ranging from inert gas overlayers on various substrates to metallic layers on metals. It is often observed when the interaction between atoms in the overlayer is of comparable strength to their interaction with the substrate. At low temperatures or pressures the overlayer lattice is commensurate with the substrate but at a critical value of T or P, arrays of domain walls are formed and cause the overlayer lattice to loose registry with the substrate [56]. Figure 6.23 shows a one dimensional example of a domain

Figure 6.23. Example of an incommensurate phase with a light domain wall.

wall marked by D. Far from the domain wall, the overlayer atoms remain in registry with the substrate, but near the wall the overlayer atoms may be shifted from registry because of their asymmetric environments. A domain wall like the one in fig. 6.23 that has lower density than the other parts of the overlayer is called a light wall. Domain walls with higher local density are called heavy walls. The domain walls may be ordered to form a domain wall

solid or disordered to form a domain wall fluid. The properties of the commensurate-incommensurate transition can be described completely in terms of the interactions between the domain walls and many variations are possible including such non-intuitive cases as a commensurate solid-to-fluid-to-incommensurate solid sequence of transitions [15,57].

6.3. DEFECTS AND THE SURFACES OF REAL MATERIALS

So far in this chapter, surfaces have for the most part been assumed to be ideal crystals and we have ignored the fact that real surfaces always contain a wide variety of defects and that these defects can significantly alter the behavior of the surface. A few of the examples already discussed illustrate this point. In the case of the Si(111)-(7 x 7) - to - (1 x 1) transition, the (7 x 7) phase nucleates and grows from the top edges of steps as already illustrated in fig. 6.18. The Au(110)-(1 x 2) surface, fig. 6.10a, is not perfectly ordered and has various types of defects including regions of (1 x 3) structure. The Si(100)(1x2) surface shown in 6.11 has numerous defects and the CO induced reconstruction in fig. 6.12 is really the image of a point defect. Defects are common.

Surface defects can take on many forms some of which are illustrated schematically in fig. 6. 24. Point defects include self- and foreign adatoms (A)

Figure 6.24. Types of surface defects. (A) Adatoms, (B) vacancies, (C), screw dislocations, (D) step edge adatoms, (E) edge dislocations, (F) step edge vacancies, (H) steps.

and vacancies (B). Steps (H) are examples of extended defects and can have their own point defects (D) and (F) that are called *kinks*. Bulk defects like edge (E) and screw (C) dislocations can intersect the surface.

Surface defects occur for many reasons. They can be intrinsic to the surface; in which case they have concentrations that are determined by thermodynamic or kinetic properties of the material. Defects can be created by thermal or mechanical stresses during fabrication of the surface. For example,

in the preparation of low index surfaces, even a slight misalignment of the crystal will introduce steps. Contamination due to impurities present in the bulk substrate or to adsorption from the gas or liquid environment is another common source of defects.

Many solids such as glasses and polymers have little or no crystallinity. Liquid surfaces also have no long range order. The concepts of surface crystallography are of little use in describing the surface properties of these highly non-crystalline materials.

6.3a. Surface Point Defects and Their Properties

Surface point defects such as vacancies and impurity atoms have significant effects on the surface properties of materials. For example, one-half monolayer of oxygen adsorbed on a clean W(112) surface below 350 K forms a random structure that orders into a (2 x 1) structure upon heating. The addition of randomly distributed nitrogen impurities drastically slows down the kinetics of ordering, breaks the long-range order of the (2 x 1) structure, and lowers the critical temperature of the (2 x 1) order-disorder transition [58]. Another example is given by adsorption of small amounts of alkali metal atoms which can not only significantly alter the structure, as already discussed, but can also change the reactivity of the surface. For example, small amounts of potassium increase the selectivity of the Fisher-Tropsch reaction towards higher molecular weight products [59].

Oxides are an good example of materials whose surface properties are strongly affected by the presence of defects [60]. The bonding in many oxides is strongly ionic and an important type of point defect is caused by removal of a surface oxygen ion. This removal creates a vacancy and the cations around it modify their positions to adjust to their changed environment. In addition, in order to maintain charge neutrality, one or two electrons become bound to the vacancy. The electronic properties in the vicinity of an oxygen vacancy are drastically altered from those of the perfect surface and this in turn changes the chemical reactivity of the surface. Many oxides are inert to adsorption of common gases like CO unless defects are present.

Free dislocations, fig. 6.25, provide another way to destroy the

Figure 6.25. Example of a dislocation pair on a square lattice.

long-range order of a layer of adsorbed atoms and are believed to play a central role in two dimensional melting of adsorbed layers [61]. A free dislocation results from the distortions created when an extra partial row of atoms is added to an ordered structure. Free dislocations interact with each other through their long-range strain fields and can also be pinned by defects on the substrate. On an infinite surface, free dislocations must always occur in pairs. Surface dislocations are also created when a bulk edge dislocation encounters the surface. Surface electronic and magnetic properties might be expected to change near a dislocation but there are no studies of this.

The energy required to form various defects like those in fig. 6.24 can be estimated from the simple nearest neighbor bond model introduced in Section 6.2a. For example, removal of an atom from the (111) surface of an fcc crystal requires that a total of nine bonds (six between neighbors in the surface layer and three with neighbors in the second layer) be broken. This requires an energy of $u_v = 9\varepsilon/2$. However, if the atom is not completely removed but only placed on top of the (111) surface as a self adatom, three new bonds are formed. Thus the energy u_s to form a vacancy - self adatom pair is only 3ε. An even smaller energy is required if the atom is placed at a step edge or at a kink site on the step edge. Since vacancy-adatom pairs increase the entropy of the surface, their equilibrium concentration will increase as the temperature increases. At low concentrations, this fraction of vacancy-adatom pairs is determined by the Boltzmann factor $e^{-3\varepsilon/kT}$. In the case of metals, ε is on the order of an electron Volt and the equilibrium concentration of point defects at room temperature will be small. However, the preparation of clean, well-ordered surfaces often involves annealing at temperatures above 1000 K where the vacancy-adatom pair concentration can be on the order of several percent. If the crystal is quenched too rapidly, this higher defect concentration will be frozen in

If the defect formation energies are known, the surface configuration at any temperature can be determined from statistical thermodynamics using Monte Carlo methods. Figure 6.26 shows a typical result for the case of a

Figure 6.26. Examples of increasing surface defect density as a function of temperature in the solid-on-solid model [62]. (Courtesy of G. H. Gilmer.)

simple cubic crystal with only nearest neighbor interactions for various values of kT/ε [62].

As the densities of various types of defects increase, interactions between them become important and the energies of defect formation become concentration dependent. One consequence is that catastrophic changes in the surface properties can occur. The roughening transition, illustrated by the simulations in fig. 6.26, is an example. At the roughening temperature, the density of steps increases dramatically and average width of the crystal-vacuum interface begins to diverge logarithmically. For open faced (11n) surfaces of fcc metals, roughening is found to occur at temperatures in the range $0.5T_m$ to $0.75T_m$.

6.3 b. Extended Surface Defects

Examples of extended surface defects include steps, grain boundaries, and screw dislocations. Until the advent of STM, steps were the only extended defects that had been extensively studied experimentally. Ordered arrays of nearly equally spaced and parallel steps can be created if a crystal surface is slightly misoriented from a low index plane. By changing the angie of misorientation, the step density can be varied. This type of slightly misoriented surface is called a *vicinal* surface and is specified by the Miller indices of the bulk planes parallel to it. Because the steps on a vicinal surface are in uniform arrays, they form a diffraction grating with translational periodicity different from the non-stepped surface. Thus, ordered step arrays are easily studied by diffraction and the average values of step height and step spacing can be directly measured. Stepped surfaces are often modeled by staircases for which the terraces or treads consist of strips of low-index surface separated by single or multiple atomic height risers.

Real steps are more complex in their structure as is easily seen in Figs.— . Step edges are not straight and, even on carefully prepared vicinal surfaces, have numerous kinks along them. Kinks increase the surface entropy and their

equilibrium density is determined thermodynamically in analogy to the spontaneous generation of point defects discussed in the preceding section.

The local environments of atoms at step edges and at kink sites along step edges are different than the environments of atoms on a perfect surface. These differences alter the electron densities and thus change the local electrical and chemical behavior of the surface. For example, the redistributed charge density at a step edge creates a local dipole moment which in turn changes the surface work function. This effect has been demonstrated on several materials [63].

Steps also have important effects on the rates of crystal growth from the vapor phase. In the case of epitaxial growth of Si on a Si(001) substrate [64], adsorbed Si atoms condense into one monolayer thick islands whose edges are atomic height steps. Island growth occurs when Si atoms that are diffusing about on the surface encounter the edge of an island and are accommodated to it. Steps running in different directions on the surface have different atomic structures. For Si(001) these differences cause the accommodation coefficient to be much higher on step edges that are perpendicular to the dimer rows of the substrate. (The dimer reconstruction is illustrated in fig. 6.11.) This causes the islands to grow very anisotropically and become much longer along the directions of dimer rows. If the growth is stopped and the surface annealed, the islands become more circular; this demonstrates that it is the kinetics of the sticking process that are different rather than differences in the energetics of adsorption at the various types of step edge sites.

In an important series of experiments, Blakely and Somorjai [65] showed that steps can strongly alter the chemical reactivity of a surface. In the case of Pt surfaces, they found that C-H and C-C bond breaking in adsorbed hydrocarbon molecules occurs preferentially on stepped (111) surfaces but not on the (111) surface itself. Steps can also cause the distribution of adsorbed atoms to be nonuniform. For example, fig. 6.27a is a photoelectron

Figure 6.27. (a) 0.2 monolayer of Cu on a slightly misoriented Mo(110)surface. The image diameter is 40 μm. (b) Step pinning caused by surface impurities on Si (111). The image is 2.6μm x 3.75 μm. (Micrographs provided courtesy of E. Bauer.)

microscope image of a 40 μm diameter region on a Mo(110) surface covered with about 0.2 monolayer of Cu, shown as the bright lines [66]. The Cu atoms are preferentially adsorbed at the bases of steps. The white arrows mark the location of a slip plane which had been induced by differential stresses caused by rapid heating of the substrate.

Impurities can also greatly alter the properties of steps on surfaces. Eizenberg and Blakely [67] studied the effects of segregation of carbon to vicinal surfaces near Ni (111). At high temperatures, the surface coverage of carbon is low and the vicinal surfaces have the expected uniform staircase structures with monoatomic height steps. Graphite precipitation begins to occur at temperatures below the equilibrium precipitation temperature, T_p. This causes the vicinal surfaces to become unstable and to break up into {111} facets. However, in the intermediate temperature range between T_p and about 1.1 T_p, a single monolayer of graphite is precipitated and, depending on the original step directions, the monoatomic step arrays are replaced by either (111) and (110) facets or by (111) and (311) facets. Such phenomena is complex and not understood from a theoretical point of view.

At high temperatures, surface diffusion causes steps to migrate across the surface to relieve localized regions of misorientation or strain. When impurities are present, step migration can be impeded. Figure 6.27b shows an example for Si(111) [66]. Surface contaminants (probably SiC precipitates, shown by the black specks) pin steps while motion far from the impurities is able to continue giving rise to complex bowed step arrays.

6.3 d. Surfaces of non-crystalline materials (polymers and composites)

The surfaces of many materials are not crystalline. Examples include glasses and polymers. Other materials which are crystalline in their equilibrium state can also be prepared in metastable states that are either amorphous of very highly polycrystalline. Prior to the development of STM and AFM, it was not possible to study the atomic scale structure of such materials. Thus, the advent of STM and AFM has opened up entire new areas of research that are only beginning to be explored.

Figure 6.28. (A) STM image of polyimide surface structure [69]. (B) 500 Å x 500 Å STM image showing strands of calf thymus DNA [71].

Figure 6.28A shows a 200 x 180 Å^2 STM image of a small ordered region on the surface of a polyimide thin film. The ridges near the center are about 32 Å apart which is repeat distance of the structural unit for this polymer.

The conformation of adsorbed biomacromolecules and their interactions on surfaces is of interest in immunology for applications such as the development of new medical diagnostic techniques [70]. These systems provide another example in which standard surface structure determination techniques are of little use. Figure 6.28B shows STM images of strands of calf thymus DNA in which the helical period of 22.8 Å is resolved [71].

6.4. TECHNIQUES FOR SURFACE STRUCTURE DETERMINATION

A wide variety of experimental techniques have been used to study surface crystal structures. It is beyond the scope of this chapter to make a detailed presentation of these techniques and the reader is referred to the extensive literature [72]. Structural techniques can be roughly divided into two basic categories: diffraction and direct.

6.4 a. Diffraction methods

The regular rows of atoms at the surface of a crystal form a diffraction grating. If the surface is illuminated by a beam of monochromatic radiation of wavelength λ. the conditions for constructive interference of the reflected radiation are given by Bragg's law

$$n\lambda = 2d\sin\theta \qquad (23)$$

where d is the spacing between equivalent rows or planes of atoms, 2θ is the angle through which the incident radiation is scattered, and n is an integer that

determines the order of the diffraction. In general $\lambda < 2d/n$ so that λ must be somewhat shorter than the d-spacings of interest. Highly collimated, monochromatic beams of atoms, electrons, and x-rays can all be prepared with the appropriate wavelengths and are the most widely used diffraction probes for practical surface crystallography. The wavelength is determined from the de Broglie relationship

$$\lambda = h/p, \qquad (24)$$

where p is the momentum and h the Planck constant. Electrons and atoms of energy E have $p^2 = 2mE$, where m is the particle mass, and photons have $p = h\nu/c$, where ν is the frequency and c the speed of light.

For an incident beam, Bragg's Law defines the directions along which diffracted beams are emitted from the sample. The directions and intensities of these beams provide the basic data needed to determine the structure of the crystal surface. Bragg's Law and the spatial pattern of the diffraction beams are sufficient to determine the size, shape, and space group of the surface unit mesh but in order to obtain the positions of the basis atoms within the unit mesh, the intensities of the diffraction beams must be analyzed. The procedures for doing this are dependent upon the detailed interaction potential between the incident particles and the surface; i. e. upon the elastic and inelastic scattering cross sections.

Atom diffraction is the most surface sensitive of all the diffraction techniques because the elastic scattering cross sections of atoms are so large that they cannot penetrate the surface at all. Instead, they are scattered from the electronic potential several angstroms outside the ion cores of the surface atoms. Since the atoms are neutral, both conducting and non-conducting surfaces can be studied. An atom must have thermal energy (a few meV) to have the appropriate wavelength for diffraction, as is easily calculated from eqn. 24.

Low energy electrons (10-500 eV) have large inelastic cross sections that restrict their penetration to only a few atomic layers into the material. Their elastic cross sections are also large; this results in high intensities in the diffracted beams so that experiments are relatively easy. For these reasons *low energy electron diffraction*, LEED, is by far the most widely used technique

for surface crystallography. A complication occurs in determination of the atomic positions because the large elastic cross sections cause the electrons to have a high probability of being scattered more than once. This *multiple scattering* complicates structure determinations. However, sophisticated, straight-forward procedures for LEED structure analysis have been developed [7] and allow atomic positions to be routinely determined to better than 0.1 Å. LEED is not generally useful for studies of non-conducting materials.

Both x-rays and neutrons have very small inelastic cross sections so that, in most situations, the part of the diffracted signal due to surface atoms is swamped by scattering from the bulk. For this reason, neutron diffraction is only used for materials such as intercalated graphite that have a large intrinsically surface to volume ratio. This would also be the case for x-rays if not for the fact that their high frequencies result in an index of refraction n_x that is slightly smaller in materials than in vacuum; i. e. $n_x = 1 - \delta_x$ where δ_x in of the order of 10^{-5}. This causes x-rays to be totally reflected if their grazing angle of incidence is smaller than the critical angle

$$\theta_c = (2\delta_x)^{1/2}. \qquad (25)$$

Typically, θ_c is less than a degree. For $\theta < \theta_c$, an evanescent wave with decay length of only a few tens of Ångstroms penetrates the surface. This shallow penetration makes grazing incident x-ray diffraction highly surface sensitive. However, the small cross sections require incident intensities that are higher than available in laboratory x-ray sources. For this reason, routine x-ray studies of surfaces can only be carried out at synchrotron radiation sources. Because of their high penetration, x-rays are also useful probes of buried interfaces.

6.4 b. Direct or geometrical methods

Several techniques yield direct information about the atomic structure of surfaces. Field Ion Microscopy (FIM) and Transmission Electron Microscopy (TEM) can obtain direct images of surface or interfacial structures with atomic scale resolution. Other techniques such as Rutherford backscattering (RBS) and medium energy ion backscattering provide direct information about

surface structure but do not yield a direct image. Spectroscopic techniques like infrared absorption, angle resolved ultra-violet photoelectron spectroscopy (ARUPS), and high resolution electron energy loss spectroscopy (HREELS) are sensitive to the vibrational modes of surface species and thus contain information about adsorption site symmetries. Because the spectroscopic techniques are sensitive to local structure, they are particularly useful for studies of non-crystalline systems.

Field ion microscopy was invented by Erwin Muller [74] and was the first technique to yield atomic resolution images of surfaces. In FIM, the image is obtained from the tip of a very sharply pointed, fine wire with a radius of a hundred Ångstroms or less. A strong electric field is applied between the tip and an imaging screen a few centimeters away. Because of the tip's small radius of curvature, the electric field near it is extremely high - several volts per Ångstrom. The highest field strengths are near surface protrusions such as step edges. An imaging gas of He or Ne is introduced into the volume around the tip. Near the tip, the electric field is strong enough to ionize atoms of the imaging gas. These positively charged ions are then accelerated away from the tip by the strong electric field and strike the imaging screen to yield an image like that in fig. 6.29. The bright spots correspond to the positions of atoms on

Figure 6.29. A field ion micrograph of a small island of adsorbed Si atoms on a W(110) surface [75]. Every Si atom is visible.

the surface of the tip. Atoms in exposed positions feel stronger electric fields and are therefore more visible - atoms near the center of planes may not be visible. The magnification achieved by FIM is on the order of one million.

6.4c. Evaluation of traditional methods.

Diffraction measurements yield statistical information about a surface structure. One reason for this is that the incident beam illuminates a large area on the surface - typically 1 mm^2 or larger - so that many atoms, including atoms at defect sites, simultaneously contribute to the signal. Thus diffraction

techniques are best utilized for crystallographic studies of surfaces with nearly ideal structures and very good long range structural order. Disorder in the surface can profoundly alter the properties of the diffraction [76]. For example, if the regions of perfect crystalline order are small with dimension L, the diffraction beams are broadened by an amount proportional L^{-1}. On a real surface , L has a distribution of sizes and, if this distribution is known, the variation of intensity within each of the diffraction beams can be calculated. For example, the angular width of the diffracted beam is determined by the mean size of the finite size regions. Unfortunately, there is no unique solution to the inverse problem, i. e. determination of the distribution function of finite size regions directly from the measured beam profile. Thus, in practice, diffraction measurements yield little more than the average size of the ordered regions.

Point defects are even more difficult to study using diffraction because they have little effect on the diffraction beams themselves. Instead, point defects contribute a weak, nearly uniformly distributed diffuse background to the diffraction pattern. The situation is even more difficult because scattering from surface phonons causes intensity from the diffracted beams to be redistributed throughout the diffraction pattern as *thermal diffuse scattering* [78]. From a practical viewpoint, it can be extremely difficult to separate the thermal diffuse scattering from the point defect scattering.

Atom diffraction is limited because it is only sensitive to the outermost layer of atoms and therefore unable to provide information about the structure in the second or deeper atomic layers. X-rays, on the other hand, can penetrate well below the surface and thus are an attractive probe to study buried interfaces. No other diffraction method offers this possibility. X-rays and atoms can also have the advantage that they can be used for crystallographic studies of insulating materials, whereas electrons and ions cannot. Because of their high penetration, X-rays can be used with high gas pressures over the sample and make it possible to study surface structures under ambient conditions. High temperature and time dependent studies are also possible.

LEED is the most highly developed method for structure determination. The capability for immediate visual display of the diffraction pattern coupled with its long history of successful use, continue to make LEED the technique most widely used to monitor surface structures including surface phase

transitions. The resolution of the best LEED instrumentation rivals that of X-ray diffractometers. Furthermore, LEED is not limited to near grazing angles of incidence.

Several electron microscopy techniques provide direct images of surface structures. Transmission electron microscopy (TEM) uses high energy electrons (~100 keV) and can be used to study the atomic structure of solid-solid interfaces, surface structure and the structure of mesoscopic particles. However, the need for special sample preparation techniques in TEM is a major barrier to wide application. Low Energy Electron Microscopy (LEEM) uses more surface sensitive electrons with several tens of eV kinetic energy. Examples of LEEM images are given in fig. 27. Neither LEEM nor the technique of reflection electron microscopy have achieved atomic resolution but they provide the capability for in situ measurements at elevated temperature in real-time. For these reasons, both are important for the study of surfaces processes at high temperatures especially when only mesoscale information is sought. Unfortunately, none these direct electron based methods is useful for studies of dielectric materials.

Ion scattering is an easily interpreted technique because of the geometrical nature of the scattering but provides only local information averaged over the entire surface. It is also relatively insensitive to defects and not useful for insulators. Ions are strongly interacting particles and in many cases radiation induced damage limits applicability. Quantitative analysis of ion scattering data is also complicated by the sensitivity to lattice vibrations.

Vibrational spectroscopies such as High Resolution Electron Energy Loss Spectroscopy (HREELS) and Infra Red (IR) absorption provide powerful information about local site geometries but are relatively insensitive to long range order or defect structures and types. IR does not require a vacuum environment over the sample and is therefore one of the only techniques that can probe the liquid-solid interface or the gas-solid interface at high pressures.

Finally, no single method has the capability to study all problems in surface structure, rather, each has a range of applications in which it is superior and often several techniques must be applied to the same system before a complete structural characterization is possible.

6.5. THE ROLE FOR STM AND AFM

The first STM images had an immense impact on surface science research simply because they demonstrated that it might be possible to directly image the atomic structure of surfaces. This potential to view the structural properties of surface defects such as vacancies, atomic height steps and domain boundaries meant that new advances in our understanding of the properties of real surfaces were at hand. Previously only field-ion microscopy and, under very special circumstances, transmission electron microscopy had demonstrated similar capabilities.

6.5 a. Strengths of STM.

The most important contributions of STM are due to its capability to image the neighborhood around individual atoms. Thus it yields direct information about point defects, local electronic structure, kinks and other step morphologies. Furthermore, STM does not require large, single crystalline samples and can therefore be used to study the local atomic structures on amorphous and polycrystalline materials. No other technique rivals STM for these types of studies.

Because of their limited lateral resolution and lack of subsurface resolution, STM and AFM are unlikely to ever rival the precision of diffraction methods for complete crystal structure determinations on well-ordered surfaces. However, STM and AFM do provide reliable information about the symmetry and size of the unit mesh and some information about vertical distortions in the surface layer. They quickly determine if the surface is well ordered, if more than one type of ordered structure is present, and if finite size effects are significant. This type of complimentary information is invaluable in eliminating incorrect models and thus providing a better defined starting point for subsequent LEED or X-ray structure determinations.

The ability to apply scanned probe techniques at the liquid-solid interface opens up whole new areas of study of important problems in adhesion and friction, microbiology, and materials processing. For amorphous materials or materials for which large single crystals do not exist, scanned probe techniques may be the best structural techniques available.

6.5 b. Limitations of STM and AFM in surface crystallography.

A few of the fundamental limitations of scanned probe methods, such as the inability of STM to image insulating materials, were apparent from the beginning. Because of the strong interaction between the tip and the surface, there is also always the potential for the surface properties to be altered by the measurement. The practitioner must therefore always be on the lookout for measurement induced artifacts. For example, when does the tip alter the surface structure? Is it always possible to uniquely separate the structural and spectroscopic content of the signal? Under what conditions are atoms transferred between the tip and the sample? When can the tip cause adatoms to move about on the surface? How can ghost images caused by tunneling at more than one point on the tip be recognized? Most of the possible artifacts are discussed in other chapters. As the theoretical understanding of STM and AFM improve these limits will become better understood and appreciated.

One of the most important limitations is that STM does not probe the subsurface structure. Thus, STM is not an effective technique to study topics such as oscillatory relaxations or subsurface reconstructions. The lateral resolution of STM is also limited by the area on the surface that contributes to the current so that atomic positions cannot be determined with the same degree of precision possible with LEED or other diffraction techniques. STM is also not able to obtain images fast enough to study the local surface structure of fluid adsorbate phases because images cannot be obtained in times short compared to diffusion times.

A final category of limitations is due to technological limits of existing instrumentation. In many cases, these will be removed or reduced in the future by improved instrumentation. One important example is that STM cannot be used to study surfaces at high temperatures because of thermal drift and because the piezoelectric drivers cease to operated above several hundred degrees. Another is the limited ability to study kinetic processes due to the relatively long times required to acquire images.

As with all other techniques used to study surface structure, STM and AFM have specific strengths and weaknesses. They cannot solve all problems

in surface structure but must be applied with skill and insight in conjunction with other complementary methods.

ACKNOWLEDGEMENTS

I especially thank M. B. Webb, M. G. Lagally and P. Kleban for invaluable discussions that have shaped many of my viewpoints about the structure of surfaces. My research in the area of surface structure has been supported by grants from the National Science Foundation and the Office of Naval Research.

REFERENCES

1. See for example Chapter 4 in **Solid State Physics**, N. W. Ashcroft and A. D. Mermin (Holt, Rinehart and Winston, New York, 1976).
2. B. K. Vainshtein, **Modern Crystallography** (Springer-Verlag, Berlin, 1981).
3. R. E. Allen and F. W. de Wette, Phys. Rev. **179**, 873 (1969).
4. H. B. Nielsen, J. N. Andersen, L. Petersen, and D. L. Adams, J. Phys. C **15**, L113 (1982); D. L. Adams, H. B. Nielsen, J. N. Andersen, I. Stensgaard, R. Friedenhans'l, and J. E. Sorensen, Phys. Rev. Lett. **49**, 669 (1982); H. L. Davis and J. R. Noonan, J. Vac. Sci. Technol. **20**, 842 (1982).
5. M. W. Finnis and V. Heine, J. Phys. F**4**, L37 (1974).
6. U. Landman, R. N. Hill, and M. Mosteller, Phys. Rev. **B21**, 448 (1980).
7. M. A. Van Hove, W. H. Weinberg, and C. M. Chan, **Low-Energy Electron Diffraction** (Springer-Verlag,Berlin, 1986).
8. C. J. Davisson and L. H. Germer, Phys. Rev. **29**, 908 (1927).
9. K. Christmann, R. J. Behm, G. Ertl, M. A. Van Hove, and W. H. Weinberg, J. Chem. Phys. **70**, 4168 (1979).
10. A. V. Titov and H. Jagodzinski, Surface Sci. **152/153**, 409 (1985).
11. H. D. Shih, F. Jona, D. W. Jepsen, and P. M. Marcus, Surface Sci. **60**, 445 (1976).
12. K. Griffiths, P. R. Norton, J. A. Davies, W. N. Unertl, and T. E. Jackman, Surface Sci. **152/153**, 374 (1985).
13. E. A. Wood, J. Appl. Phys. **35**, 1306 (1964).
14. R. L. Park and H. H. Madden, Surface Sci. **11**, 188 (1968).
15. W. N. Unertl, M. Golze, and M. Grunze, Prog. Surface Sci. **22**, 101 (1987).
16. Surface Crystallography Information Service, Eds. J. M. MacLaren, J. B. Pendry, P. J. Rous, D. K. Saldin, G. A. Somorjai, M. A. Van Hove, and D. D. Vvedensky (D. Reidel Publ. Co, Dordrecht, 1987).
17. M. A. Van Hove, R. J. Koestner, P. C. Stair, J. P. Birberian, L. L. Kesmodell, I. Bartos, and G. A. Somorjai, Surface Sci. **103**, 189,218 (1981).
18. C. M. Chan, M. A. Van Hove, and E. D. Williams, Surface Sci. **91**, 440 (1980); D. L. Adams, H. B. Nielsen, M. A. Van Hove, and A. Ignatiev, Surface Sci. **104**, 47 (1981).
19. L. D. Mark, Surface Sci. **139**, 281 (1984).
20. I. K. Robinson, Y. Kuk, and L. C. Feldman, Phys. Rev. **B29**, 4762 (1984).
21. M. Guillope and B. Legrand, Surface Sci. **215**, 577 (1989).

22. S. M. Foiles, Surface Sci. **191**, L779 (1987).
23. K. M. Ho and K. P. Bohnen, Phys. Rev. Lett. **59**, 1833 (1987).
24. R. M. Tromp, R. J. Hamers, and J. E. Demuth, Phys. Rev. B **34**, 5343 (1986).
25. W. A. Harrison, **Electronic Structure and the Properties of Solids** (W. H. Freeman and Co., San Francisco, 1980).
26. T. Gritsch, D. Coulman, R. J. Behm, and G. Ertl, Phys. Rev. Lett. **63**, 1086 (1989).
27. K. H. Rieder, M. Baumberger, and W. Stocker, Phys. Rev. Lett. **51**, 1799 (1983).
28. B. E. Hayden, K. C. Prince, P. J. Davie, G. Paolucci, and A. M. Bradshaw, Solid State Comm. **48**, 325 (1983); M. Copel, W. R. Graham, T. Gustafsson, and S. Yalisove, Solid State Comm. **54**, 695 (1985).
29. H. C. Potter and J. M. Blakely, J. Vac. Sci. Technol. **12**, 635 (1975); T. M. Buck, G. H. Wheatley, and L. Marchut, Phys. Rev. Lett. **51**, 43 (1983).
30. Some general references are: N. D. Lang, Solid State Phys. **28**, 225 (1973); F. Forstmann in **Photoemission and the Electronic Properties of Surfaces**, Eds. B. Feuerbacher, B. Fitton, and R. F. Willis (John Wiley, New York, 1978) p. 193; J. E. Inglesfield, Repts. Prog. Phys. **45**, 223 (1982).
31. G. A. Somorjai, **Principles of Surface Chemistry** (Prentice-Hall, Englewood Cliffs,1972).
32. J. M. Blakely, **Introduction to the Properties of Crystal Surfaces** (Pergamon, Oxford, 1973).
34. A. Pavlovska, K. Faulian, and E. Bauer,Surface Sci. **221**, 233 (1989).
35. A. R. Kortan and R. L. Park, Phys. Rev. **B23**, 6340 (1981).
36. J. S. Ochab, G. Akinci, and W. N. Unertl, Surface Sci. **181**, 452 (1987).
37. D. Menzel, in **Kinetics of Interface Reactions**, Eds. M. Grunze and H, J, Kreuzer (Springer-Verlag,Berlin, 1987) p.2 and references therein.
38. T. L. Einstein in **Chemistry and Physics of Solid Surfaces IV**, Eds. R. Vaneslow and R. Howe (Springer-Verlag, Berlin, 1983).
39. E. A. Guggenheim, **Thermodynamics** (North-Holland, Amsterdam, 1988) p. 33.
40. N. Osakabe, K. Yagi, and G. Honjo, Japan J. Appl. Phys. **19**, L309 (1980).
41. M. Schick, Prog. Surface Sci. **11**, 245 (1981); C. Rottman, Phys. Rev. **B24**, 1482 (1981).
42. P. Kleban in **Chemistry and Physics of Solid Surfaces V**, Eds. R. Vaneslow and R. Howe (Springer-Verlag, Berlin,1984) p. 339.

43. L. E. Reickl, **A Modern Course in Statistical Physics** (University of Texas Press, Austin, 1980).
44. R. J. Birgeneau and P. M. Horn, Science **232**, 329 (1986).
45. C. Kittel, **Introduction to Solid State Physics** (Wiley, New York, 1986).
46. J. C. Campuzano, M. S. Foster, G. Jennings, R. F. Willis, and W. N. Unertl, Phys. Rev. Lett. **54**, 2684 (1985).
47. L. D. Landau and E. M. Lifshitz, **Statistical Physics, Part I** (Pergamon Press, Oxford, 1980) p. 459-471; I. P. Ipatova and Y. E. Kitaev, Prog. Surface Sci. **18**, 189 (1985).
48. H. E. Stanley, **Introduction to Phase Transitions and Critical Phenomena** (Oxford, United Kingdom, 1971).
49. W. N. Unertl, Comments Cond. Mat. Phys. **12**, 289 (1986).
50. P. Bak, Solid State Commun. **32**, 581 (1979).
51. J. F. van der Veen and J. W. M. Frenken, Surface Sci. **178**, 382 (1986).
52. F. F. Abraham, Phys. Rev. **B23**, 6145 (1981).
53. J. D. Weeks in **Ordering in Strongly Fluctuating Condensed Matter Systems**, Ed. T. Riste (Plenum, New York, 1980) p. 293.
54. I. K. Robinson, E. H.Conrad, and D. S. Reed, J. de Phys. Paris **51** (in press 1990).
55. F. C. Frank and J. H. van der Merwe, Proc. Roy. Soc. London Ser. A **198**, 205 (1949).
56. D. R. Nelson and B. I. Halperin, Phys. Rev. **19**, 2457 (1979).
57. R. J. Birgeneau, G. S. Brown, P. M. Horn, D. E. Moncton, and P. W. Stephens, J. Phys. C **14**, L49 (1981); F. F. Abraham, S. W. Koch, and W. E. Rudge, Phys. Rev. Lett. **49**, 1830 (1982).
58. J. K. Zuo, G. C. Wang, and T. M. Lu, Phys. Rev. B40, 524 (1989).
59. D. J. Dwyer in **Physics and Chemistry of Alkali Metal Adsorption**, Eds. H. P. Bonzel , A. M. Bradshaw, and G. Ertl (Elsevier, New York, 1989) p. 307.
60. V. E. Henrich, Prog. Surface Sci. **14**, 175 (1983); R. J. Lad and V. E. Henrich, J. Vac. Sci. Technol. **A6**, 781 (1988); M. Tsukada, H. Adachi, and C. Satoko, Prog. Surface Sci. **14**, 113 (1983).
61. K. J. Strandburg, Rev. Mod. Phys. **60**, 161 (1988).
62. H. J. Leamy, G. H. Gilmer, and K. A. Jackson in **Surface Physics of Materials**, Ed. J. M. Blakely (Academic Press, New York, 1975) p. 121.
63. K. Besocke, B. Krahl-Urban, and H. Wagener, Surface Sci. **68**, 39 (1977).
64. Y. W. Mo, R. Kariotis, B. S. Swartzentruber, M. B. Webb, and M. G. Lagally, J. Vac. Sci. Technol. **B8**, 232 (1990).
65. D. W. Blakely and G. A. Somorjai, J. Catal. **42**, 181 (1976).

66. Courtesy of E. Bauer, Technical Univ. of Clausthal.
67. M. Eizenberg and J. M. Blakely, J. Chem. Phys. **71**, 3467 (1979).
68. Produced by Koch Membranes Systems, Wilmington, MA.
69. M. Grunze, W. N. Unertl, S. Gnanarajan, and J, French, Mat. Res. Soc. Symp. Proc. **108**, 198 (1988).
70. J. C. Andle, J. F. Vetelino, R. Lec, and D. McAllister, Proc. IEEE Ultrasonics Symp, (1989) p. 579
71. G. Lee, P. G. Arscott, V. A. Bloomfield, and D. F. Evans, Science **244**, 475 (1989).
72. Descriptions of the techniques discussed in this section can be found in the following references: G. Ertl and J. Kuppers, **Low-Energy Electrons and Surface Chemistry** (Verlag Chemie, Weinheim, 1974); W. N. Unertl, Appl. Surface Sci. 11/12, 64 (1982); **Electron Spectroscopy for Surface Analysis**, Ed. H. Ibach (Springer-Verlag, Berlin, 1977); G. Margaritondo, **Introduction to Synchrotron Radiation** (Oxford Univ. Press, Oxford, 1988); **Refelection High-Energy Electron Diffraction and Reflection Electron Imaging of Surfaces**, Eds. P. K. Larsen and P. J. Dobson (Plenum Press, New York, 1988).
73. A. Guinier, **X-ray Diffraction** (Freeman, San Francisco, 1963) p. 2.
74. E. W. Muller, Z. Physik **131**, 136 (1951).
75. R. Casanova and T. T. Tsong in **Thin Films and Interfaces**, Eds. P. S. Ho and K. N. Tu (Elsevier North-Holland, New York, 1982) p. 41.
76. M. G. Lagally in **Chemistry and Physics of Solid Surfaces IV**, Eds. R. Vaneslow and R. Howe (Springer-Verlag, Berlin, 1983) p. 281.
77. M. B. Webb and M. G. Lagally, Solid State Phys. **28**, 301 (1973).
78. D. E. Clark, W. N. Unertl, and P. H. Kleban, Phys. Rev. **B34**, 4379 (1986).
79. L. D. Roelofs, A. R. Kortan, T. E. Einstein, and R. L. Park, Phys. Rev. Lett. **46**, 1465 (1981).
80. G. C. Wang and T. M. Lu, Phys. Rev. **B31**, 5918 (1985).
81. I. F. Lyuksyutov and A. G. Fedorous, Soviet Phys. JETP **53**, 1317 (1981).
82. D. E. Taylor, E. D. Williams, R. L. Park, N. C. Bartelt, and T. L. Einstein, Phys. Rev. **B32**, 4635 (1985).
83. P. Piercy and H. Pfnur, Phys. Rev. Lett. **59**, 1124 (1987).
84. J. D. Todd and J. B. Pethica, J. Phys.; Condens. Matter **1**, 9823 (1989); U. Landman, W. D. Luedtke, N. A. Burnham, and R. J. Coulton, Science **248**, 454 (1990); S. Ciraci, A. Baratoff, and I. P. Batra, Phys. Rev. B **41**, 2763 (1990).

TABLE I

Universality Classes in Two Dimensions

[After reference 41]

Universality Class	α	β	γ	ν	Allowed Lattice Types				
					Oblique or Rectangular	Centered - Rectangular or Square	Triangular	Honeycomb	Honeycomb in Crystal Field
Ising	0	1/8	7/4	1	(2 x 1) (1 x 2) c(2 x 1)	c(2 x 2)		(1 x 1)	
XY with Cubic Anisotropy	Non-universal				(2 x 2) (1 x 2) (2 x 1)				
Three State Potts	1/3	1/9	13/9	5/6			(√3 x √3)		(√3 x √3)
Four State Potts	2/3	1/12	7/6	2/3			(2 x 2)	(2 x 2)	(2 x 2)
Heisenberg with Cubic Corner Anisotropy	0	1.8	7/4	1				(2 x 2)	

TABLE II

Measured Values of the Critical Exponents

Surface System	α	β	γ	ν	T_C(K)	References
Au(110) (1 x 2)	0 ± 0.2	0.13 ± 0.02	1.75 ± 0.03	1.02 ± 0.02	650-695	46,78
Ni(111)p(2 x 2)-O		0.14 ± 0.02	1.9 ± 0.2	0.9 ± 0.1	427	35,79
W(112)p(2 x 2)-O		0.13 ± 0.01	1.79 ± 0.14	1.09 ± 0.11	900	80
W(110)(2 x 1)-H		0.13 ± 0.06				81
W(110)(2 x 2)-H		0.25 ± 0.07				81
Ag(100)c(2 x 2)-Cl		0.12 ± 0.04				82
Ru(0001)p(2 x 2)-O	0.60 ± 0.04	0.085 ± 015	1.08 ± 0.07	0.68 ± 0.03	754 ± 0.6 K	83

FIGURE CAPTIONS

Figure 6.1. Structural models of low index surfaces of fcc and bcc crystals. The unfilled circles represent atoms in the surface layer, the lightly shaded circles are atoms in the second layer, and the dark circles are atoms in the third layer. The arrows indicate directions in each surface.

Figure 6.2. The five two dimensional Bravais Lattices. The angle β should always chosen to be greater than 90°.

Figure 6.3. The (100) surface of a crystal with the NaCl structure. The primitive unit mesh is outlined in the upper left corner.

Figure 6.4. The Finnis-Heine model for surface contraction. (a) The surface created by maintaining the bulk charge distribution around each ion at the surface. Each square is a bulk Wigner-Seitz cell. (b) Redistribution of the conduction electrons to smooth the surface. The ion cores are still in their bulk locations. (c) Inward displacement of the ion cores to a position of equilibrium.

Figure 6.5. Examples of ordered overlayer structures. (a) Ni(111)-(2 x 2)-H. (b) Ti(100)-(1 x 3)-O. (c)Ti(001)-(1 x 1)-N.

Figure 6.6. Examples of overlayer unit meshes. (a) $(\sqrt{5} \times \sqrt{5})R(26.57)$ on a square substrate; (b) $c(2 \times 2)$ or $(\sqrt{2} \times \sqrt{2})R(45)$ on a square lattice; (c) A (2,1;0,2) structure with no Wood equivalent.

Figure 6.7. Various types of adsorption sites on the low index fcc and bcc surfaces of fig. 6.1. The black dots represent adsorbed atoms. Sites labeled OT are on-top adsorption. Hollow sites with high symmetry are indicated by H. Bridge sites are indicated by B if all possible sites are the same, otherwise there are long-bridge LB and short-bridge SB sites depending on the relative distance between the substrate atoms.

Figure 6.8. A (1.5, 0; 0.5, 1) structure. The adsorbate molecules occupy both on-top and short-bridge sites.

Figure 6.9. Comparison of bond lengths for surface structures (arrows) with ranges of bond lengths found in bulk compounds and molecules (boxes). (After reference 7).

Figure 6.10. A ball model of the Au(110)-(1 x 2) reconstruction. (After reference 20). Arrows indicate the direction of shifts from singular positions.

Figure 6.11. An STM image of the Si(100)-(2 x 1) reconstruction [24]. Each number along the side marks a row of dimers. A unit mesh of the reconstructed surface is also shown. The surface region shown also has numerous defects.

Figure 6.12. The STM image on the left shows a "hole" induced in the reconstructed Pt(110)-(1 x 2) surface by the adsorption of CO [26]. The CO molecule is not visible in the image. A ball model is shown on the right.

Figure 6.13. γ(hkl) for lead at several temperatures [33]. The data are normalized to γ(111).

Figure 6.14. Scanning electron micrographs of a small Pb crystal. (a) Near its melting point; T = 599 K [34]. The larger flat facets are {111} surfaces and the smaller ones are {100} surfaces. (b) A slightly larger crystal showing the increase in surface topographical structures that occurs at lower temperature; T = 373 K. (Courtesy of A. Pavlovska).

Figure. 6.15. Equilibrium phase diagram for O-Ni(111) [35].

Figure 6.16. (a) The equilibrium phase diagram for Se-Ni(100) [36]. (b) Structure of the p(2 x 2) phase. (c) Structure of the c(2 x 2) phase The solid circles are Ni atoms and the open circles are Se atoms. (d) Interactions between Se atoms at various separations.

Figure 6.17. Temperature dependence of the Gibbs free energy G and the enthalpy H for (A) a first-order phase transition and (B) a second order phase transition.

Figure 6.18. (a) Coexisting regions of (7 x 7) and (1 x 1) phases on a slightly stepped Si(111) surface [40]. The dark areas are (7 x 7) and the light regions are (1 x 1). (b) Schematic illustration of the structure along the line AB in (a). (Courtesy of K. Yagi.)

Figure 6.19. (a) Two symmetry equivalent domains of a (2 x 1) structure on a square lattice. The domain boundary is marked by the dashed line. (b) The surface Brillouin zone for (a). The substrate reciprocal mesh vectors are $\mathbf{a}_1^*$ and $\mathbf{a}_2^*$. The zone center is at Γ. The reciprocal lattice vectors $\mathbf{k}_1$ and $\mathbf{k}_2$ describe the order parameters of the two (2 x 1)

domains. The wave vector **q** describes the order parameter of a c(2 x 2) structure.

Figure 6.20. Effect of the critical exponents on the diffraction at a second order phase transition [49]. The upper portion shows I_{LRO} and the amplitude of the susceptibility $\chi(0,t)$. The lower portion shows the angular profiles of diffraction beams just below, at, and just above T_c.

Figure 6.21. Critical behavior of the Au(110)-(1 x 2) order-disorder transition [46]. The upper graph corresponds to the upper portion of fig. 6.20 and shows the temperature dependence of I_{LRO} and $\chi(0, T)$. The lower curve show ln-ln plots of I_{LRO}, $\chi(0, t)$, and $\Delta S_{\|}(1/2)$ which are used to determine the critical exponents in Table II.

Figure 6.22. A molecular dynamics simulation for a two-dimensional slab showing trajectories of the atoms [52]. The bulk melting point is $T_m = 0.415\varepsilon/k$. The upper panel is just below T_m and the lower panel is just above T_m. (Courtesy of F. Abraham.)

Figure 6.23. Example of an incommensurate phase with a light domain wall.

Figure 6.24. Types of surface defects. (A) Adatoms, (B) vacancies, (C), screw dislocations, (D) step edge adatoms, (E) edge dislocations, (F) step edge vacancies, (H) steps.

Figure 6.25. Example of a dislocation pair on a square lattice.

Figure 6.26. Examples of increasing surface defect density as a function of temperature in the solid-on-solid model [62]. (Courtesy of G. H. Gilmer.)

Figure 6.27. (A) 0.2 monolayer of Cu on a slightly misoriented Mo(110)surface. The image diameter is 40 μm. (B) Step pinning caused by surface impurities on Si (111). The image is 2.6μm x 3.75 μm. (Micrographs provided courtesy of E. Bauer.)

Figure 6.28. (A) STM image of polyimide surface structure [69]. (B) 500x500 $Å^2$ STM image showing strands of calf thymus DNA [71].

Figure 6.29. A field ion micrograph of a small island of adsorbed Si atoms on a W(110) surface [75]. Every Si atom is visible.

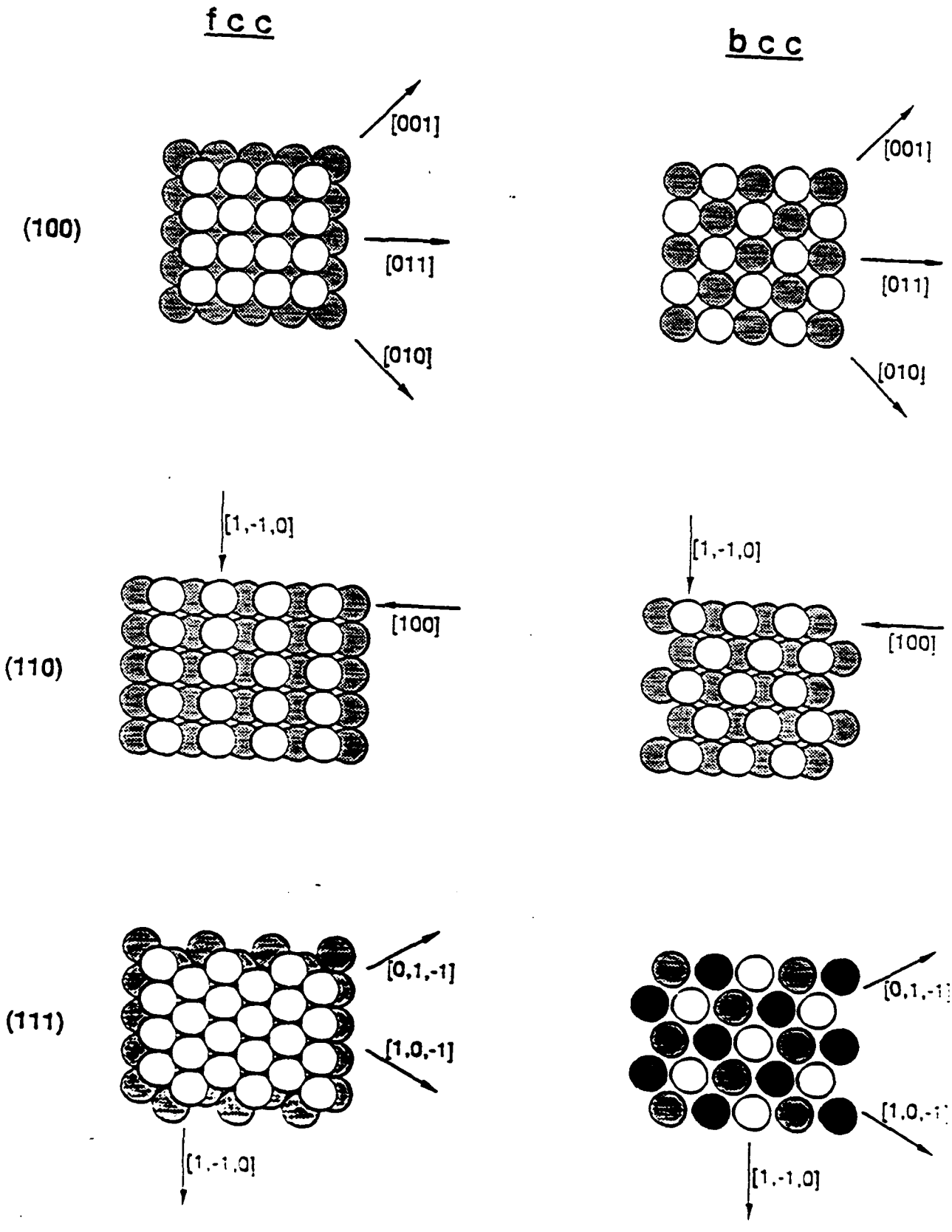
fcc
bcc
(100)
[001]
[011]
[010]
[001]
[011]
[010]
(110)
[1,-1,0]
[100]
[1,-1,0]
[100]
(111)
[0,1,-1]
[1,0,-1]
[1,-1,0]
[0,1,-1]
[1,0,-1]
[1,-1,0]

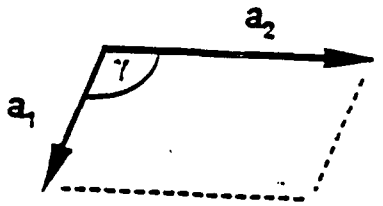

OBLIQUE

$|a_1| = |a_2|$; $90° < \gamma < 120°$

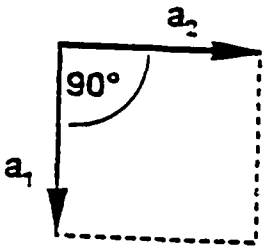

SQUARE

$|a_1| = |a_2|$

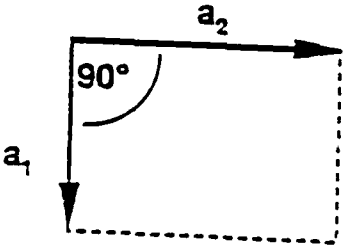

RECTANGULAR

$|a_1| = |a_2|$

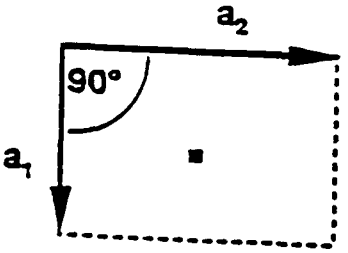

CENTERED RECTANGULAR

$|a_1| = |a_2|$

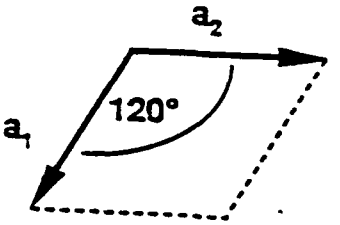

HEXAGONAL

$|a_1| = |a_2|$

FIG 6.2, LINER-

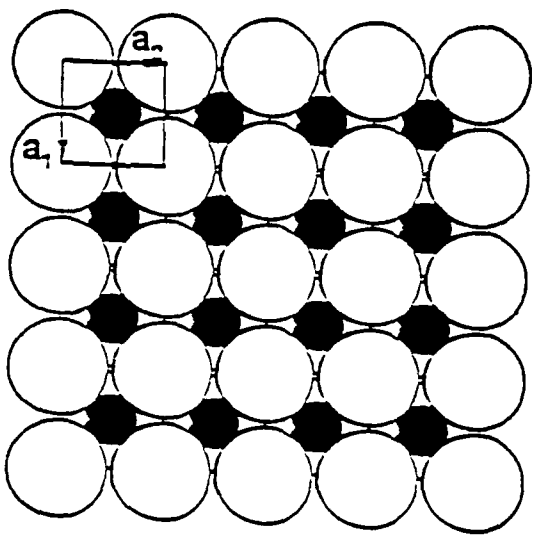

FIG 6.3, UNE:L-

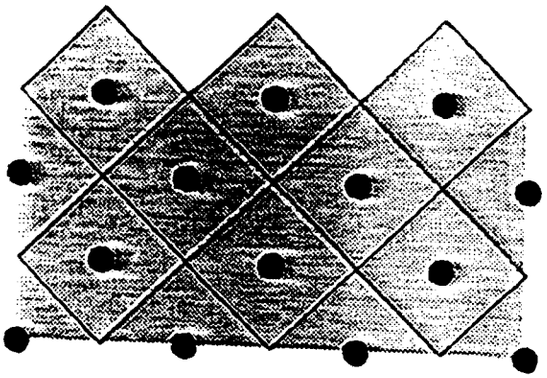

a

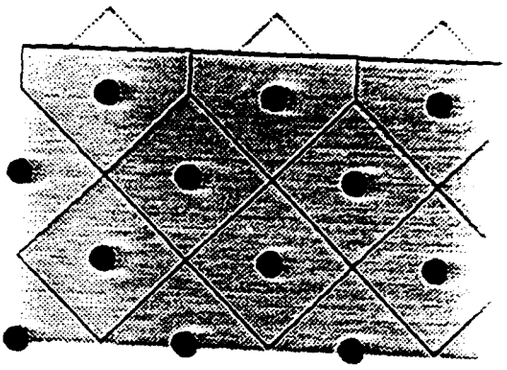

b

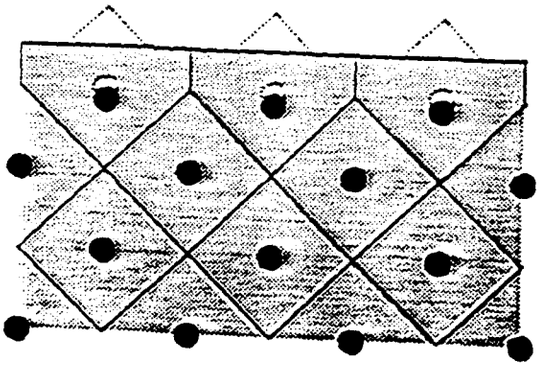

c

Fig 6.4 une

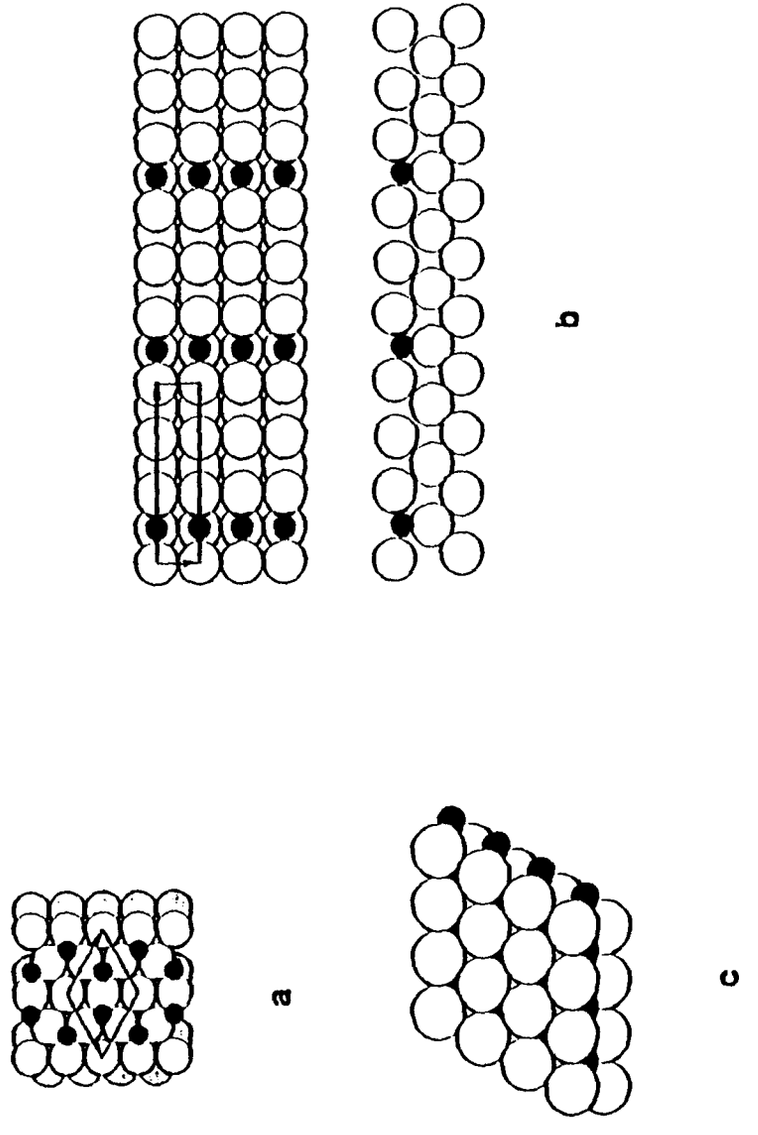

FIG 6.5, UNRELL

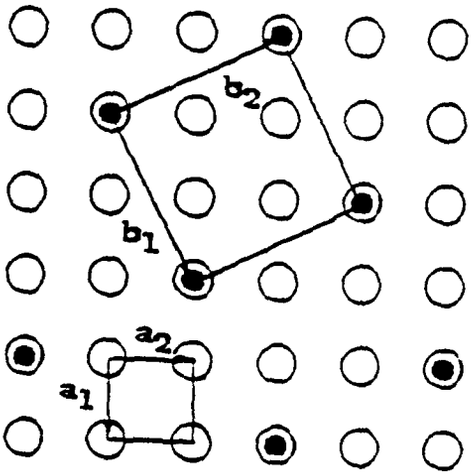

(√5 x √5)R26.57

a

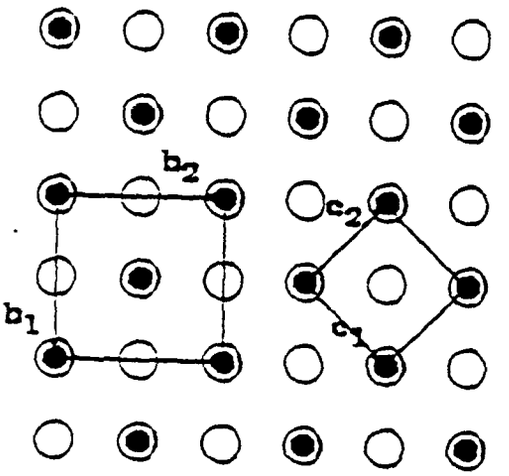

c(2 x 2) or (√2 x √2)R45

b

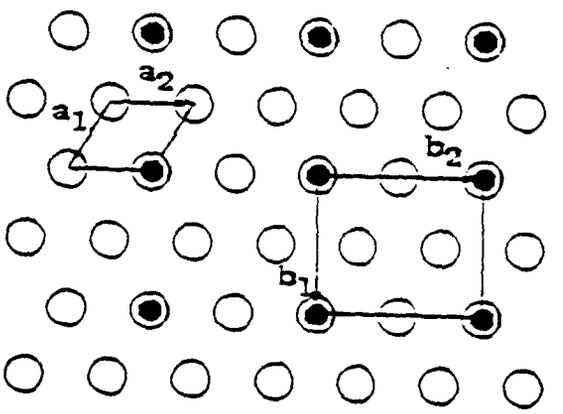

(2, 1; 0,2)

c

FIG 6.6, UNE

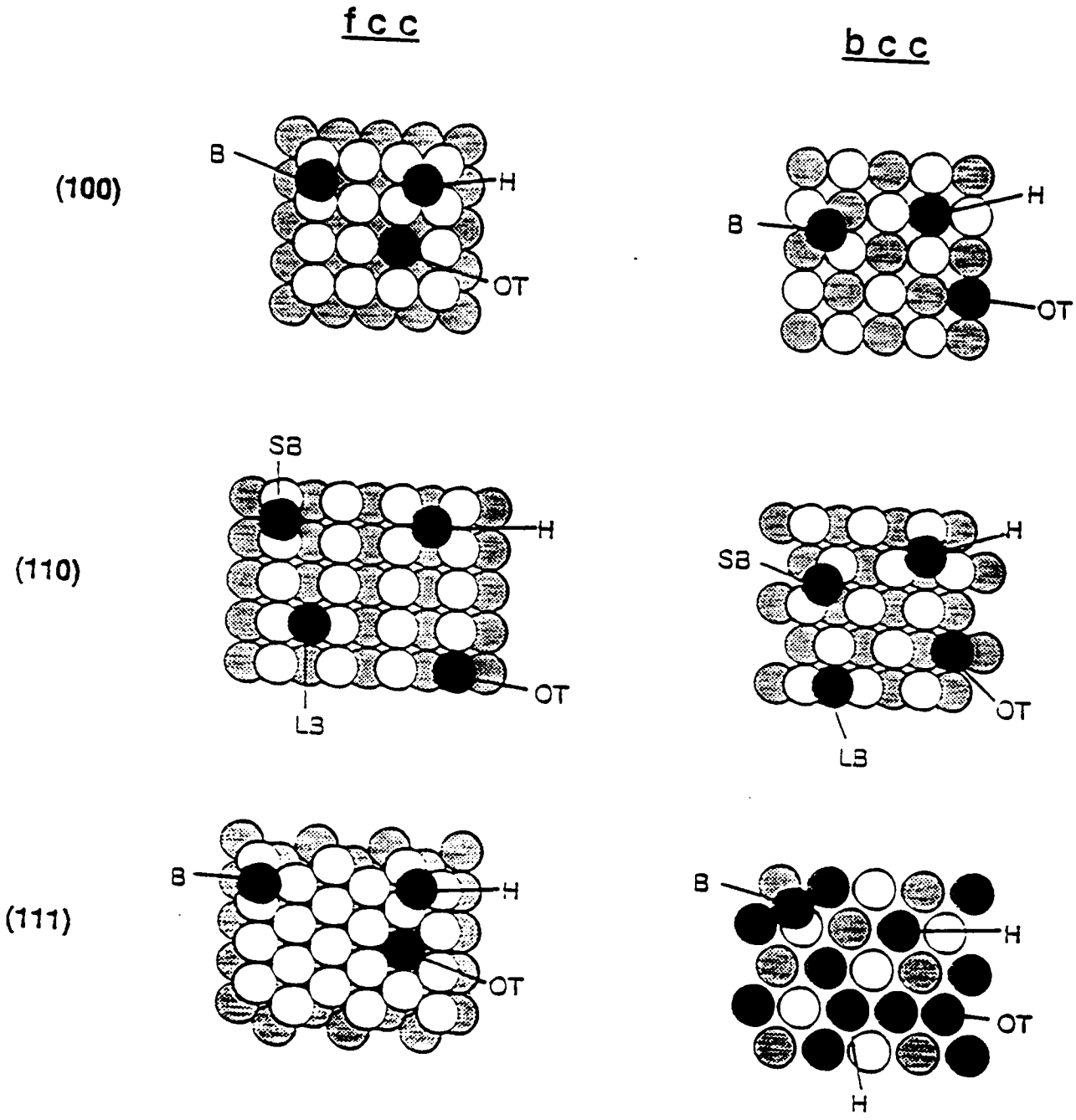

FIG. [illegible] ANERTL

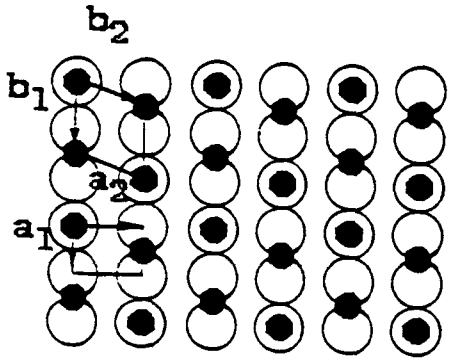

(1.5, 0; 0.5, 1)

FIG 6.8, UNERTL

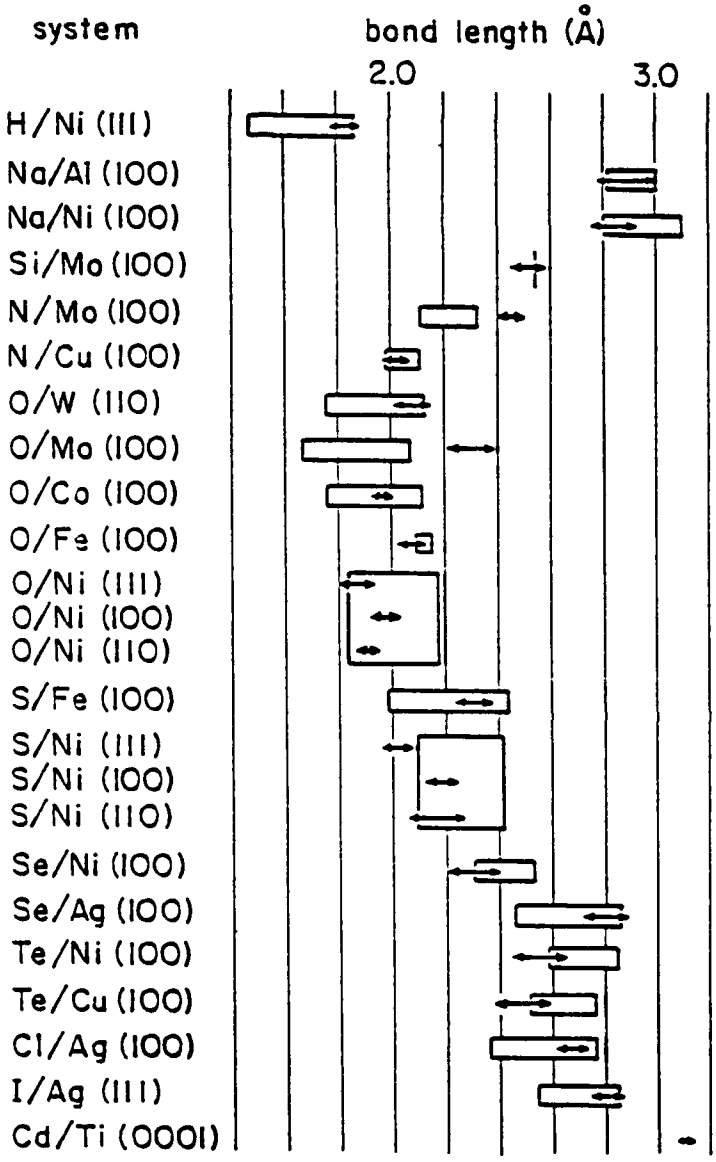

Fig 6.9, UNERTL

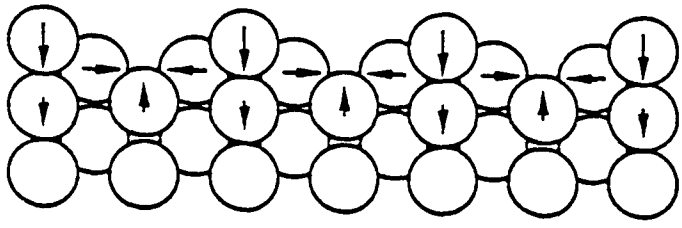

FIG 6.10, UNERTL

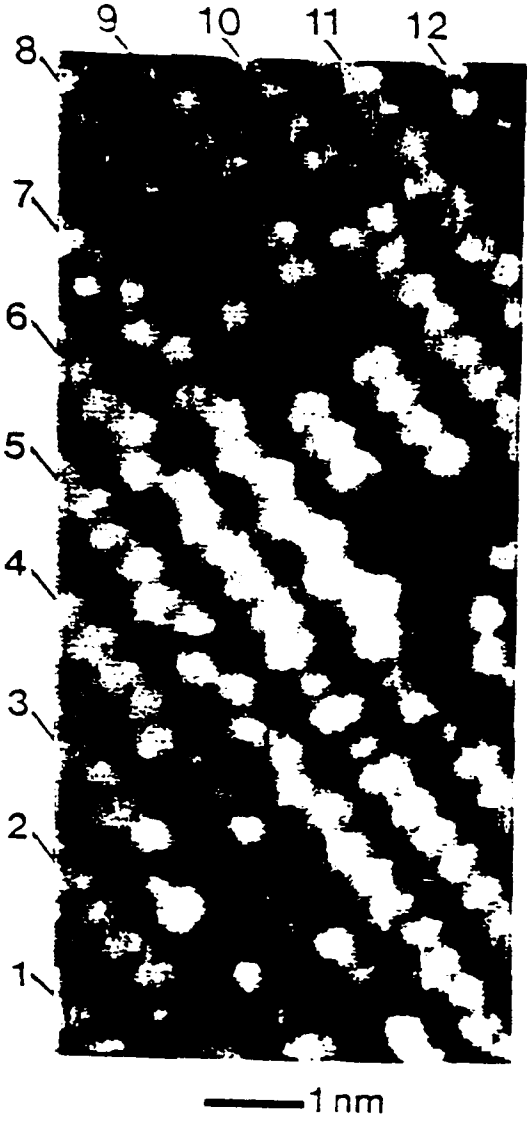
9
10
11
12
8
7
6
5
4
3
2
1
1 nm

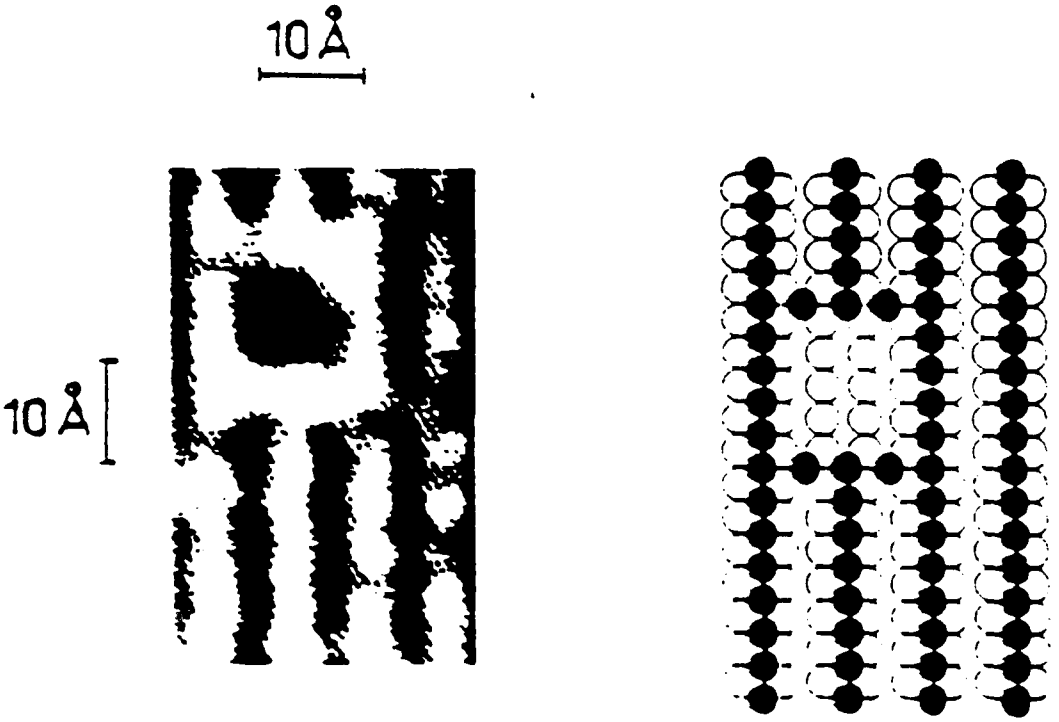
10 Å
10 Å

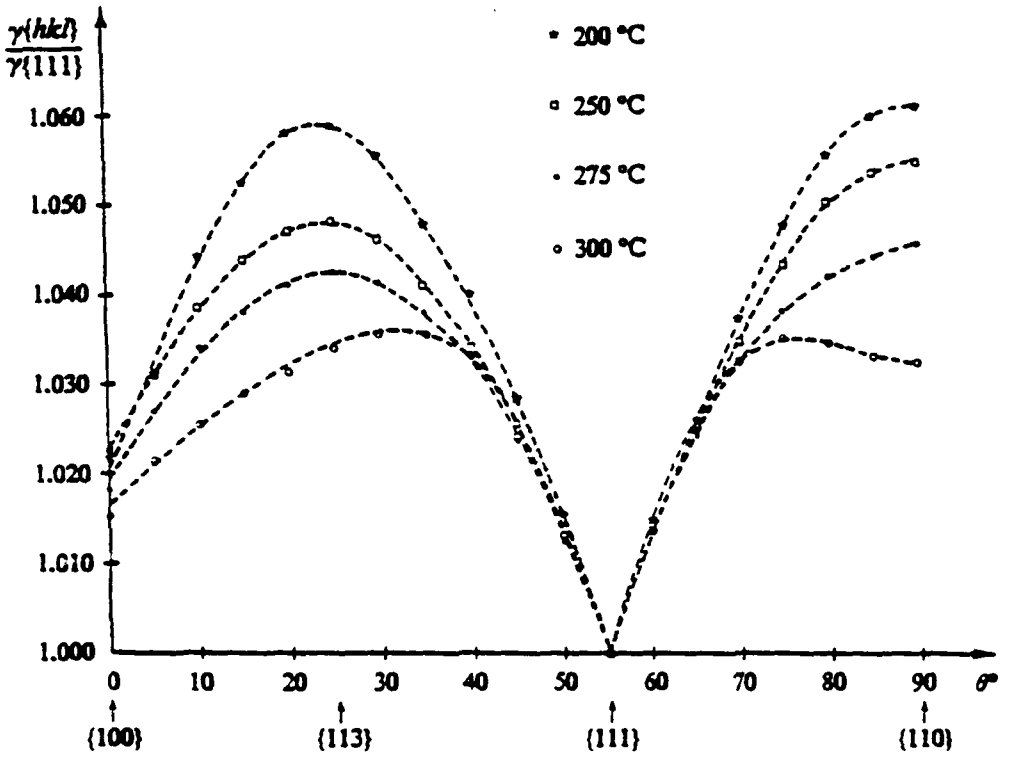
γ{hkl}/γ{111}
200 °C
250 °C
275 °C
300 °C
1.060
1.050
1.040
1.030
1.020
1.010
1.000
0
10
20
30
40
50
60
70
80
90
θ°
{100}
{113}
{111}
{110}

FIG. 6 (B) INSET

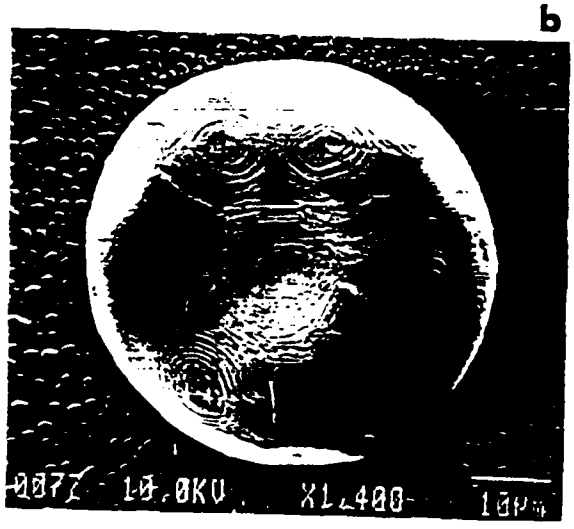

FIG 6.14
UNERTL

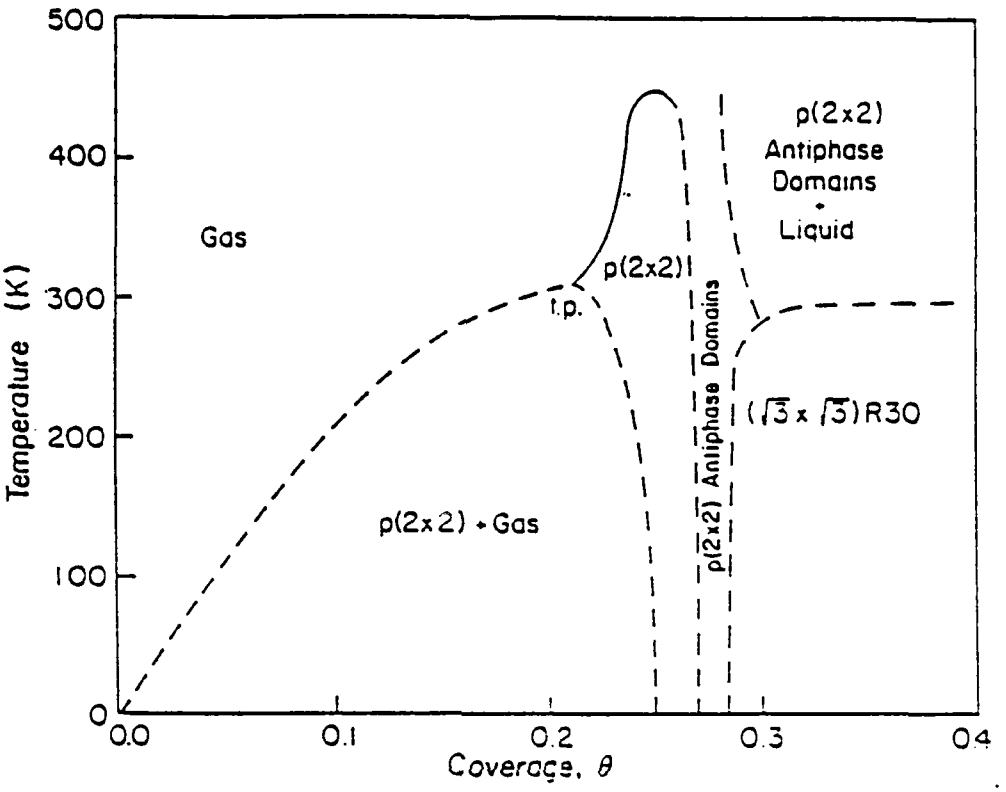
500
400
300
200
100
0
Temperature (K)
Gas
p(2x2)
Antiphase
Domains
Liquid
p(2x2)1
t.p.
p(2x2) Antiphase Domains
(√3 x √3)R30
p(2x2) + Gas
0.0
0.1
0.2
0.3
0.4
Coverage, θ

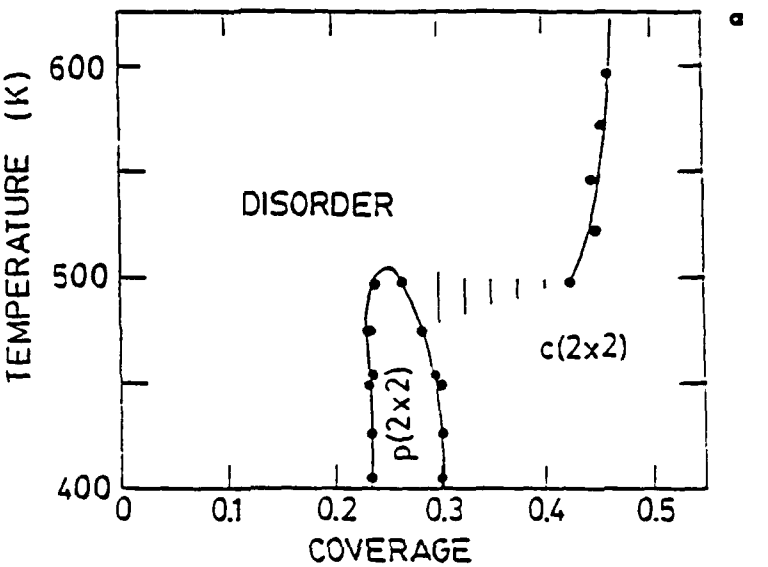
a
600
500
400
TEMPERATURE (K)
DISORDER
c(2x2)
p(2x2)
0
0.1
0.2
0.3
0.4
0.5
COVERAGE

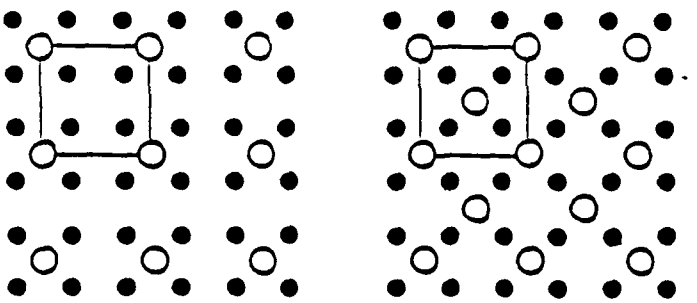
p(2x2)
b
c(2x2)
c

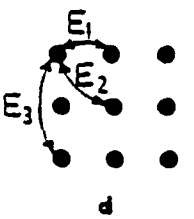
E1
E2
E3
d

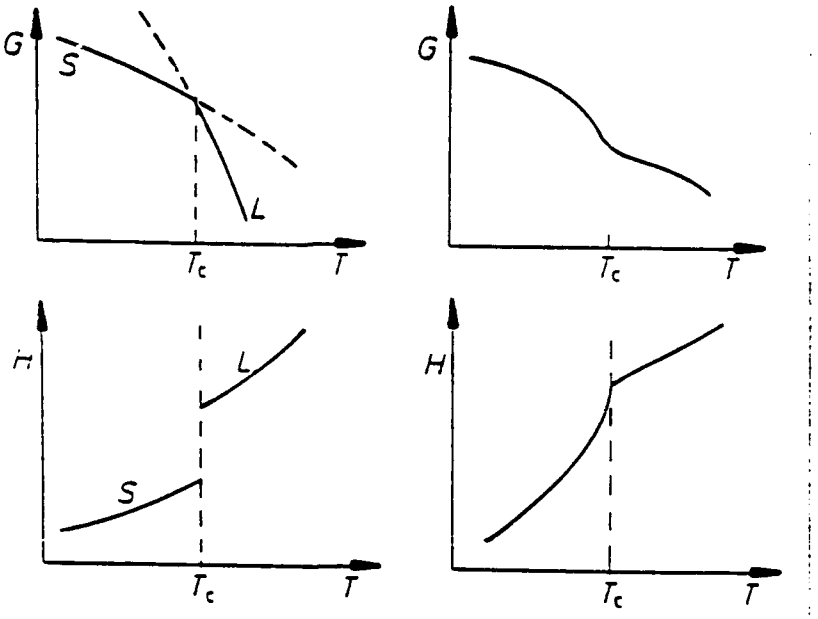
G
S
L
T_c
T
G
T_c
T
H
L
S
T_c
T
H
T_c
T
A
B

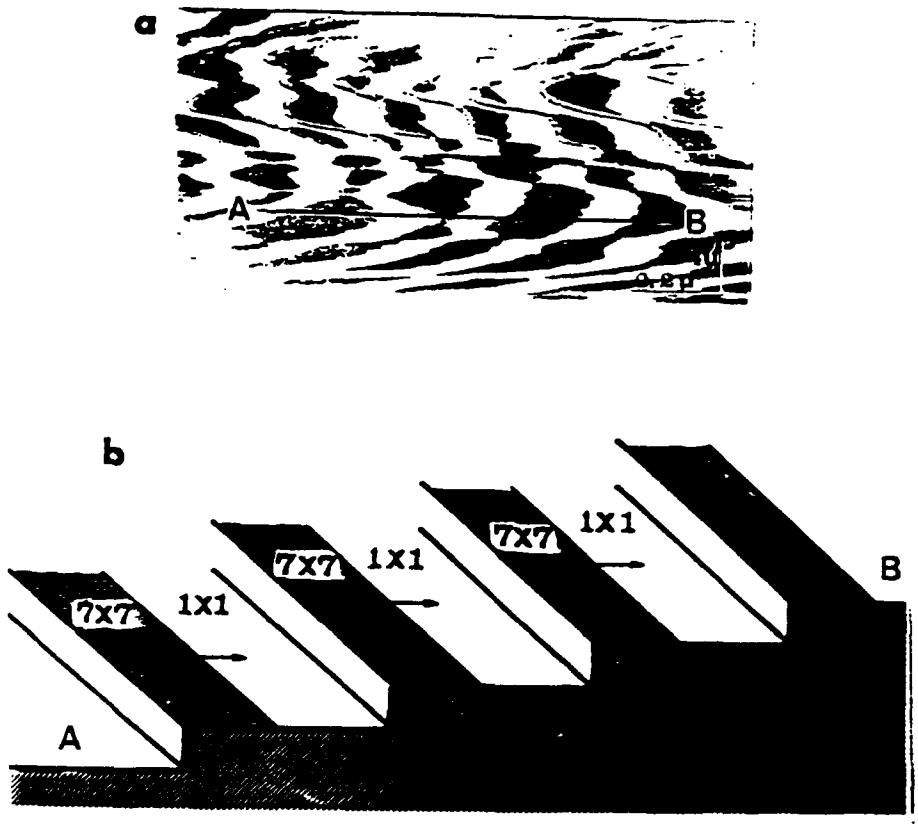

FIG. 6.18
UNERTL

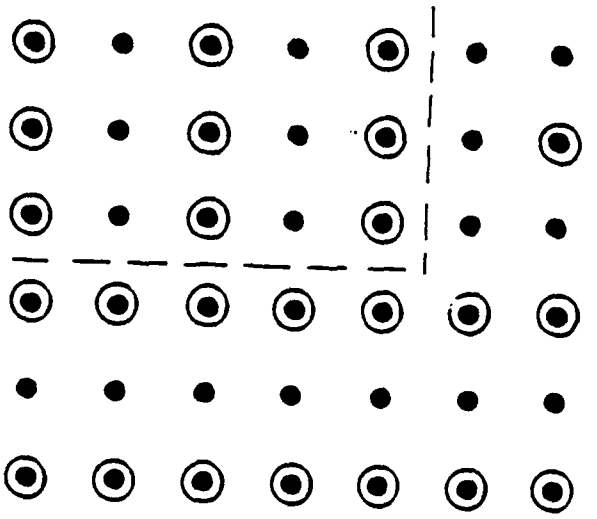

Two Domains (2x1)
(a)

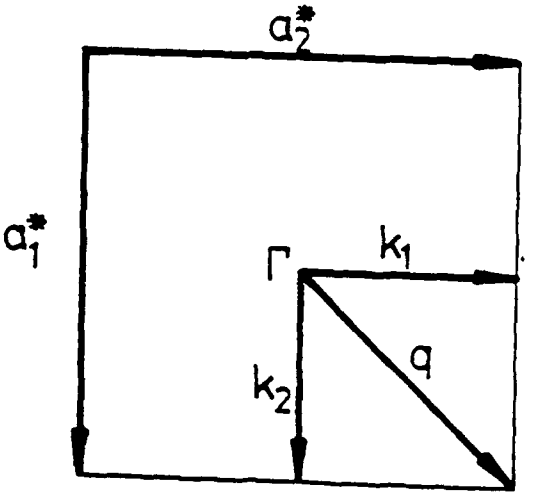

(b)

FIG 6.19, INSERT

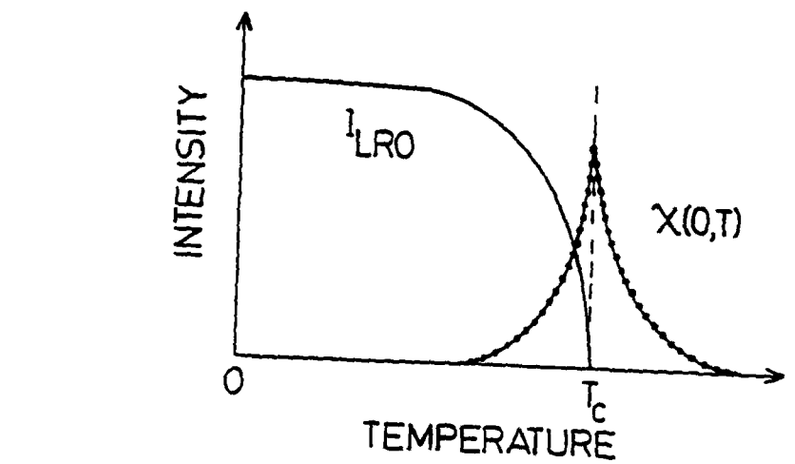
INTENSITY
I_{LRO}
$\chi(0,T)$
0
T_c
TEMPERATURE

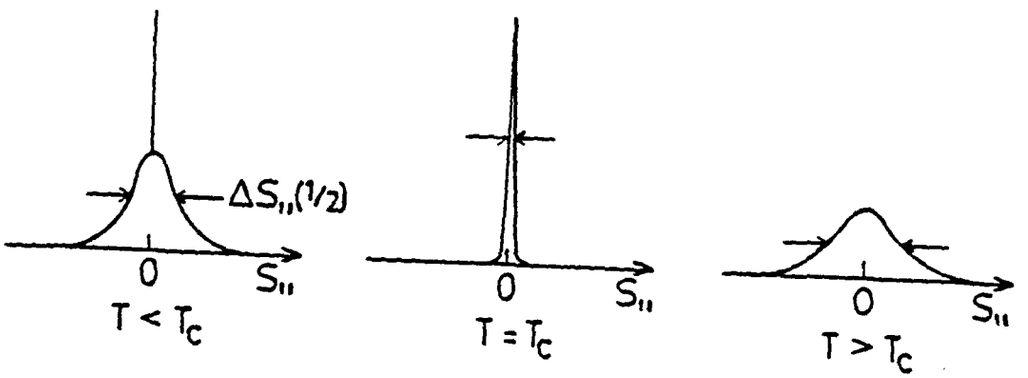
$\Delta S_{\parallel}(1/2)$
0
$S_{\parallel}$
$T < T_c$
0
$S_{\parallel}$
$T = T_c$
0
$S_{\parallel}$
$T > T_c$

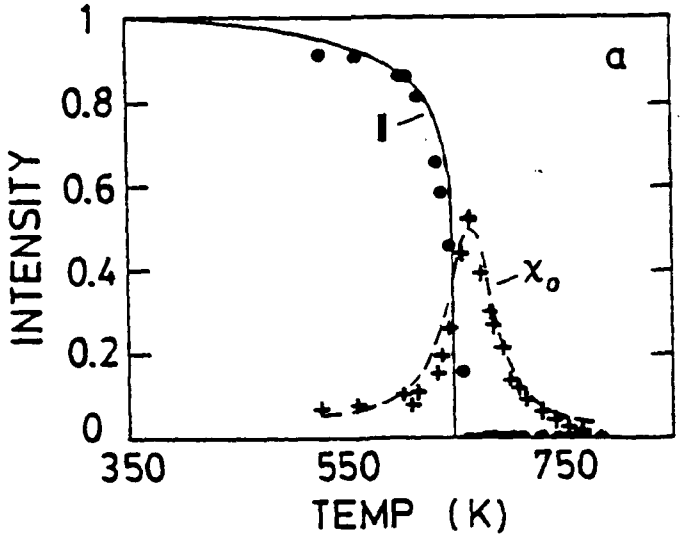

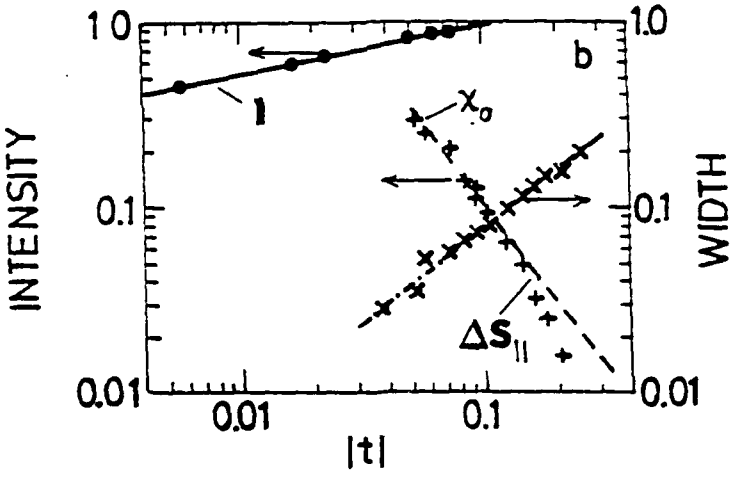

Fig 5.21, UNERTL

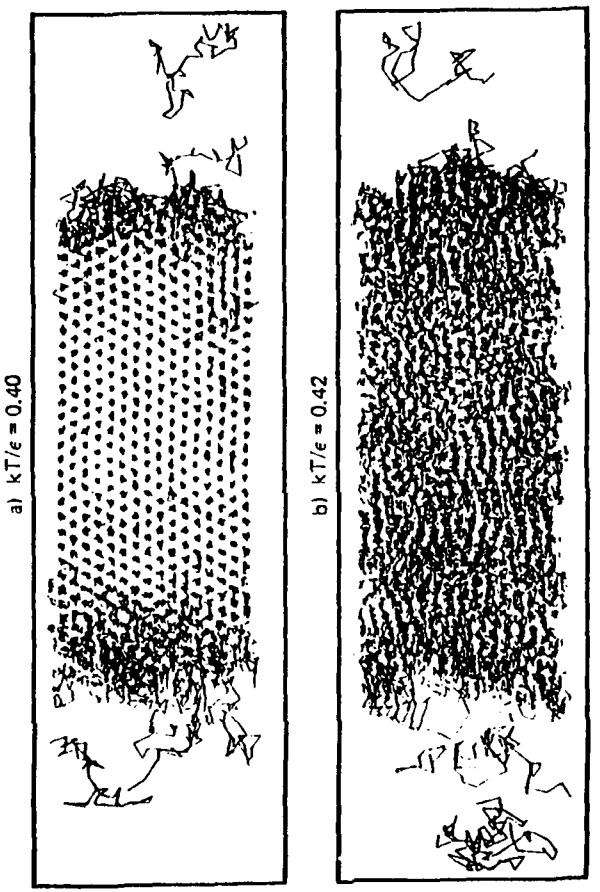

FIG 6.22, UNERTL

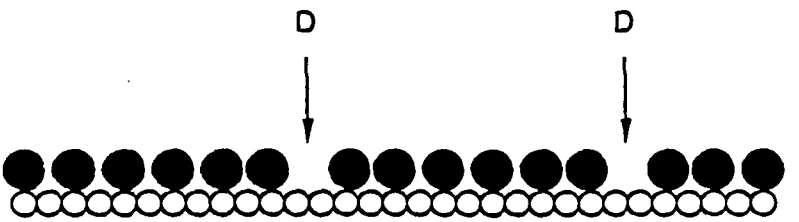

FIG 6.23, UNERTL

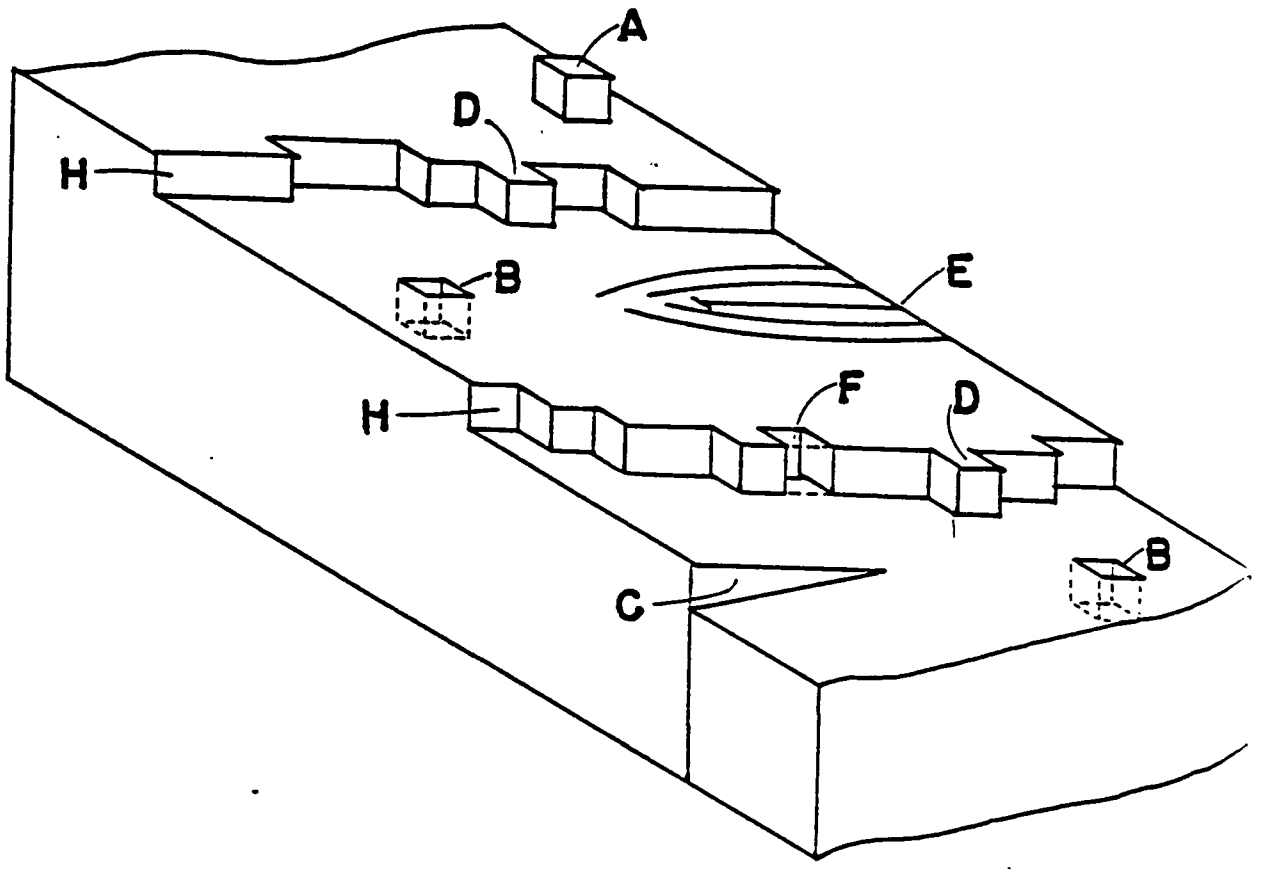

FIG. 6.24, UNERTL

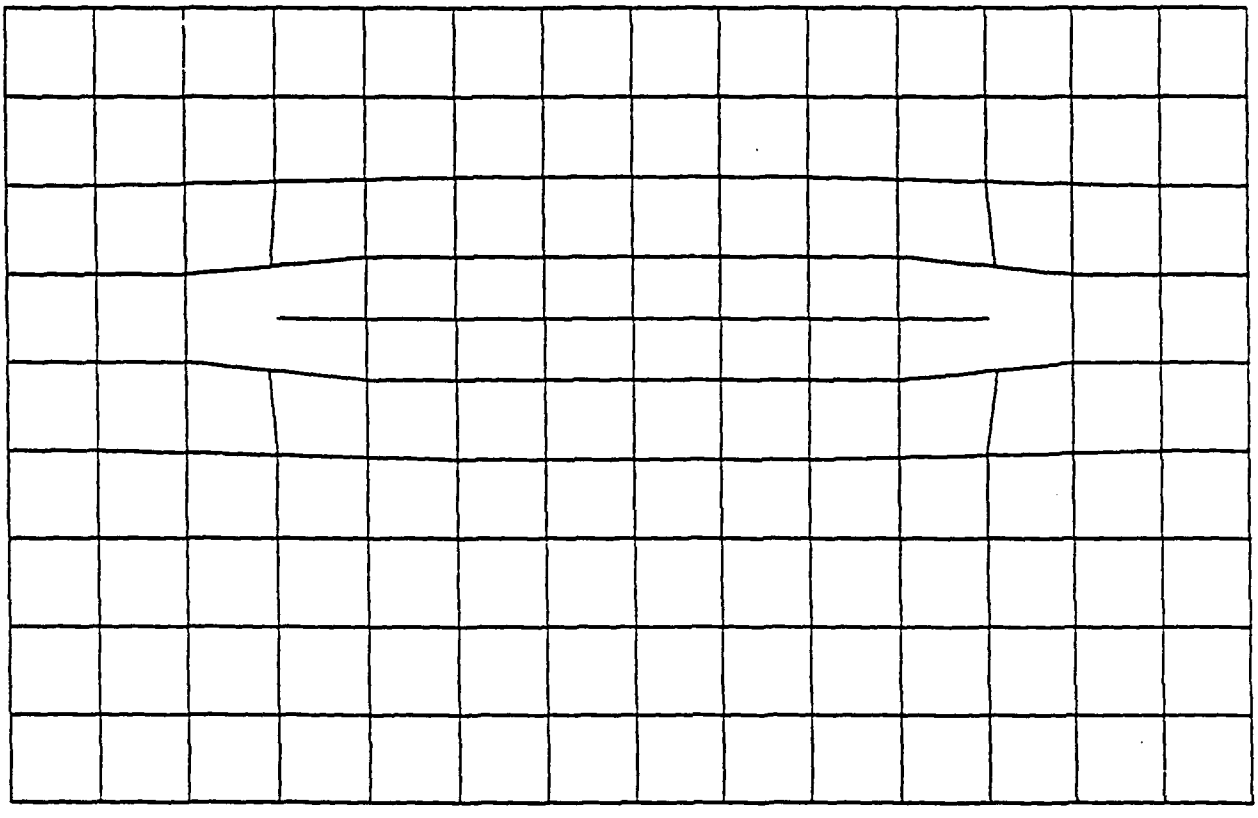

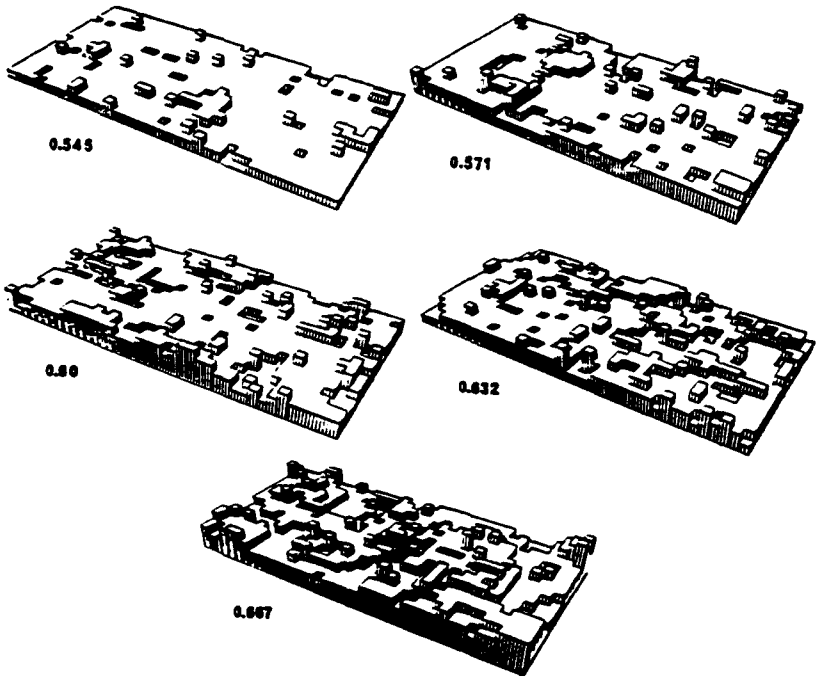

FIG 6-26, UNERTL

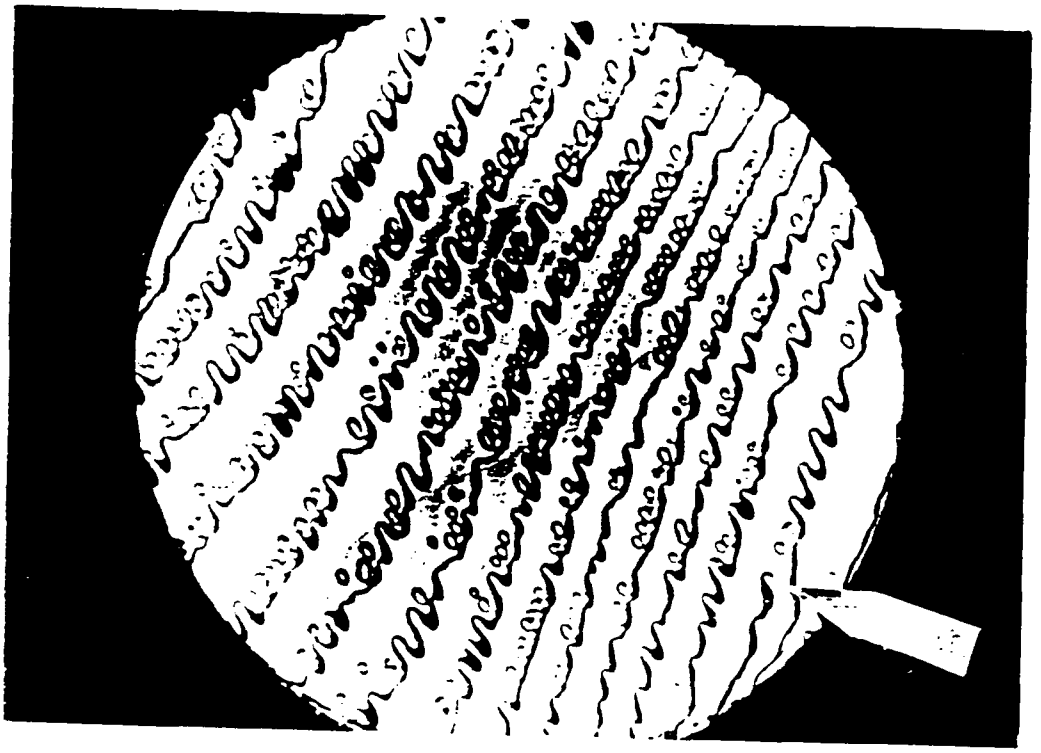

A

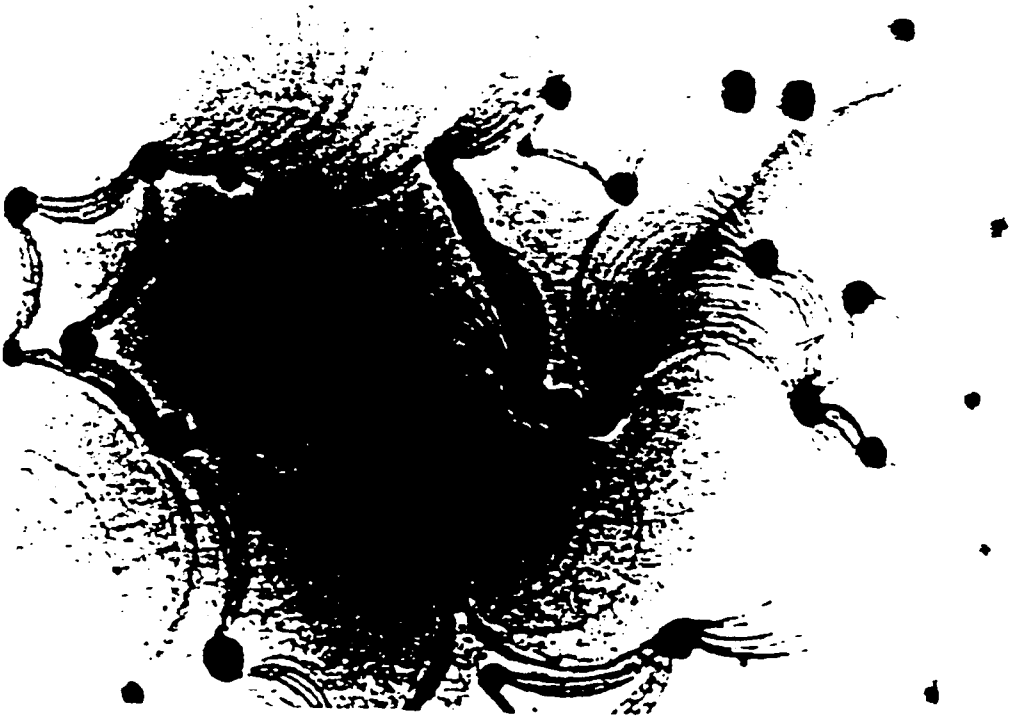

B

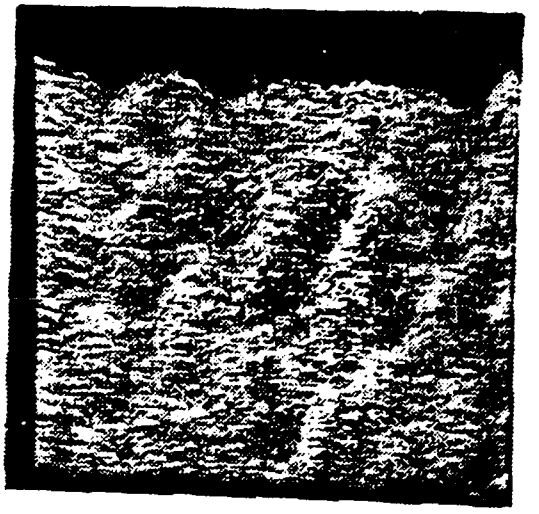

A

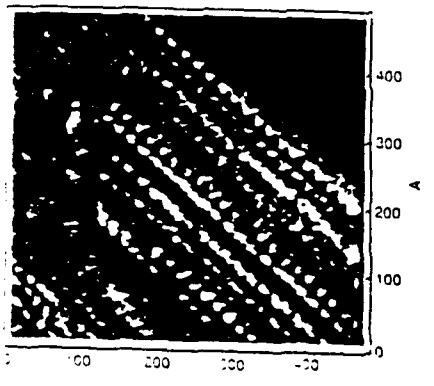

B

TECHNICAL REPORT DISTRIBUTION LIST - GENERAL

Office of Naval Research (2)
Chemistry Division, Code 1113
800 North Quincy Street
Arlington, Virginia 22217-5000

Commanding Officer (1)
Naval Weapons Support Center
Dr. Bernard E. Douda
Crane, Indiana 47522-5050

Dr. Richard W. Drisko (1)
Naval Civil Engineering Laboratory
Code L52
Port Hueneme, CA 93043

David Taylor Research Center (1)
Dr. Eugene C. Fischer
Annapolis, MD 21402-5067

Dr. James S. Murday (1)
Chemistry Division, Code 6100
Naval Research Laboratory
Washington, D.C. 20375-5000

Dr. Robert Green, Director (1)
Chemistry Division, Code 385
Naval Weapons Center
China Lake, CA 93555-6001

Chief of Naval Research (1)
Special Assistant for Marine Corps Matters
Code 00MC
800 North Quincy Street
Arlington, VA 22217-5000

Dr. Bernadette Eichinger (1)
Naval Ship Systems Engineering Station
Code 053
Philadelphia Naval Base
Philadelphia, PA 19112

Dr. Sachio Yamamoto (1)
Naval Ocean Systems Center
Code 52
San Diego, CA 92152-5000

Dr. Harold H. Singerman (1)
David Taylor Research Center
Code 283
Annapolis, MD 21402-5067

Defense Technical Information Center (2)
Building 5, Cameron Station (high quality)
Alexandria, VA 22314